EGAS MONIZ SCHOOL of HEALTH & SCIENCE | INSTITUTO UNIVERSITÁRIO EGAS MONIZ

INSTITUTO UNIVERSITÁRIO EGAS MONIZ

MESTRADO EM TECNOLOGIAS LABORATORIAIS EM CIÊNCIAS FORENSES

EVALUATION OF FUNGAL GROWTH DYNAMICS IN FOOD REMAINS UNDER INDOOR CONDITIONS FOR FORENSIC TEMPORAL ESTIMATION

Trabalho submetido por

Camila Maria Rossi

para a obtenção do grau de Mestre em Tecnologias Laboratoriais em Ciências Forenses

novembro de 2025

EGAS MONIZ SCHOOL of HEALTH & SCIENCE | INSTITUTO UNIVERSITÁRIO EGAS MONIZ

INSTITUTO UNIVERSITÁRIO EGAS MONIZ

MESTRADO EM TECNOLOGIAS LABORATORIAIS EM CIÊNCIAS FORENSES

EVALUATION OF FUNGAL GROWTH DYNAMICS IN FOOD REMAINS UNDER INDOOR CONDITIONS FOR FORENSIC TEMPORAL ESTIMATION

Trabalho submetido por

Camila Maria Rossi

para a obtenção do grau de **Mestre** em Tecnologias Laboratoriais em Ciências Forenses

Trabalho orientado por

Prof. Doutora Helena Barroso

e coorientado por

Prof. Doutor Paulo Mascarenhas e Prof. Doutora Zoé Vaz da Silva

novembro de 2025

Aos que me ensinaram a persistir.
Às raízes que me sustentam e às asas que me impulsionam.
Ao meu avô Alceu,
à minha avó Alvete,
ao meu pai Gilmar,
à minha mãe Susana,
ao meu esposo Paulo,
que, sob muito sol, me fizeram chegar até aqui na sombra.
Esta conquista é, verdadeiramente, de todos vocês.

Agradecimentos

Em primeiro lugar, sou grata à Universidade Egas Moniz, pela estrutura, recursos e todo o suporte proporcionado, que tornaram possível a realização deste trabalho.

Agradeço ao meu orientador, professor Paulo, por toda a paciência, por me incentivar e auxiliar em cada etapa deste trabalho, orientando-me com sabedoria e dedicação. À professora Zoé, o meu sincero obrigada por todos os conselhos, disponibilidade e ajuda ao longo do processo, assim como à professora Helena, por estar sempre acessível e pronta a esclarecer dúvidas.

Agradeço ainda a todas as pessoas que, de alguma forma, contribuíram para o meu crescimento académico e pessoal, e a todas as amizades que aqui fiz. Em especial, deixo um agradecimento às minhas grandes amigas Aline e Viviana, que levarei para a vida.

Por fim, gostaria de expressar a minha mais profunda gratidão à minha família. Apesar da distância e de tantas ausências inevitáveis ao longo destes anos, nunca deixaram de me fazer sentir acompanhada. Cada mensagem, cada chamada e cada palavra de incentivo chegavam sempre na hora certa, lembrando-me de que, mesmo longe, eu tinha um porto seguro à espera.

Obrigada por compreenderem as minhas escolhas, por apoiarem este caminho que tantas vezes me levou para longe e por nunca deixarem que a saudade se transformasse em obstáculo. O vosso amor deu-me força para seguir, mesmo quando a rotina apertava e o mundo parecia grande demais.

Sou profundamente grata por tudo o que fizeram, pelo apoio financeiro e emocional, pela confiança, pela paciência e pela certeza silenciosa de que eu iria conseguir. O meu agradecimento será sempre maior do que qualquer palavra possa traduzir.

A todas e todos, o meu mais sincero obrigada.

Declaração de Honra

Código | IMP-EM-EI-111_01

Declaro, por minha honra, que o presente trabalho académico é original e foi elaborado por mim próprio (a), não se tendo recorrido a quaisquer outras fontes, para além das indicadas, usadas, adotadas literalmente ou adaptados a partir dos seus originais (em fontes impressas, não impressas ou na internet) e encontram-se adequados, identificados e citados, com observância das convenções do trabalho académico em vigor.

Mais declaro que esta Tese Assessment of fungal and bacterial succession and growth patterns in food remains in indoor environments as forensic temporal markers não foi apresentada, para efeitos de avaliação, a qualquer outra entidade ou instituição, para além da(s) diretamente envolvida(s) na sua elaboração, e que os conteúdos das versões impressa e eletrónica são inteiramente coincidentes.

Declaro, igualmente, encontrar-me ciente de que a inclusão, neste texto, de qualquer falsa declaração terá consequências legais.

Data: 21/11/2025

EGAS MONIZ SCHOOL of HEALTH & SCIENCE | INSTITUTO UNIVERSITÁRIO EGAS MONIZ

Declaração Conflito de Interesses (DCI)

Código | IMP-EM-EI-110_01

Eu Camila Maria Rossi, referente a Tese Assessment of fungal and bacterial growth patterns in food remains in indoor environments as forensic temporal markers declaro que não possuo conflitos de interesse de ordem pessoal, comercial, académica, político ou financeiro.

Data: 21/11/2025

Declaração de Financiamento

Código | IMP-EM-EI-113_01

Eu Camila Maria Rossi, referente a Tese Assessment of fungal and bacterial succession and growth patterns in food remains in indoor environments as forensic temporal markers declaro que o meu trabalho não se encontra financiado.

Resumo

A estimativa do intervalo pós-mortem (PMI) permanece um desafio central na ciência forense, especialmente em ambientes fechados, onde métodos clássicos — como a avaliação de sinais cadavéricos e a entomologia — são limitados pela ausência de insetos e pela relativa estabilidade do microclima. Neste contexto, o estudo do crescimento fúngico surge como uma alternativa promissora, dado que os fungos seguem padrões temporais previsíveis durante a decomposição de restos alimentares.

Este estudo investiga a utilização de restos alimentares comuns (bananas maduras e sopas preparadas) como substratos-modelo para identificar padrões de colonização microbiana potencialmente úteis na estimativa do PMI. Avaliaram-se os efeitos da temperatura, da humidade e do estado inicial do substrato, recorrendo a observações em ambiente doméstico e a ensaios com temperatura controlada em algumas bananas — complementados por análises laboratoriais morfológicas e moleculares.

Foram identificados perfis distintos de colonização: nas sopas predominaram *Cladosporium cladosporioides, Meyerozyma caribbica* e *Penicillium citrinum*, enquanto nas bananas ocorreu o domínio de *Fusarium verticillioides*, após estágio inicial de colonização por leveduras, seguido pelo crescimento de fungos filamentosos. A relação entre área de crescimento e tempo foi modelada através de técnicas de machine learning (*ridge, elastic net polinomiais, gradient boosting e random forest*), que revelaram boa precisão para intervalos curtos (≈24–72 h), sobretudo em espécies com crescimento estável, como *P. citrinum*, e menor desempenho em casos mais variáveis, como *F. verticillioides*.

Os resultados mostram que temperatura e humidade são determinantes para o ritmo de colonização; ensaios com temperatura controlada em algumas bananas permitiram reduzir a incerteza e aumentar a precisão dos modelos preditivos. Apesar das limitações, os dados sugerem que restos alimentares podem funcionar como "relógios microbianos" complementares em ambientes fechados, contribuindo para a reconstrução da cronologia de eventos e reforçando o potencial da microbiologia forense na estimativa do PMI.

Palavras-chave: Intervalo pós-mortem (PMI), Microbiologia forense, Restos alimentares, Marcadores cronológicos.

Abstract

Estimating the post-mortem interval (PMI) remains a central challenge in forensic science, especially in closed environments, where classical methods—such as the assessment of cadaveric signs and entomology—are limited by the absence of insects and the relative stability of the microclimate. In this context, the study of fungal growth emerges as a promising alternative, given that fungi follow predictable temporal patterns during the decomposition of food remains.

This study investigates the use of common food remains (ripe bananas and prepared soups) as model substrates to identify patterns of microbial colonisation that are potentially useful in estimating PMI. The effects of temperature, humidity, and initial substrate condition were evaluated using observations in a domestic environment and temperature-controlled tests on some bananas—complemented by morphological and molecular laboratory analyses.

Distinct colonisation profiles were identified: *Cladosporium cladosporioides*, *Meyerozyma caribbica* and *Penicillium citrinum* predominated in soups, while *Fusarium verticillioides* dominated in bananas, after an initial stage of colonisation by yeasts, followed by the growth of filamentous fungi. The relationship between growth area and time was modelled using machine learning techniques (ridge, elastic net polynomials, gradient boosting and random forest), which revealed good accuracy for short intervals (≈24–72 h), especially in species with stable growth, such as *P. citrinum*, and lower performance in more variable cases, such as *F. verticillioides*.

The results show that temperature and humidity are determinants of the rate of colonisation; temperature-controlled trials on some bananas reduced uncertainty and increased the accuracy of predictive models. Despite limitations, the data suggest that food waste can function as complementary “microbial clocks” in closed environments, contributing to the reconstruction of the chronology of events and reinforcing the potential of forensic microbiology in estimating PMI.

Key-words: Post-mortem interval (PMI), Forensic microbiology, Food remains, Chronological markers

Table of contents

List of figures

List of tables

List of abbreviations

AFT – Accelerated Failure Time

CFU – Colony Forming Units

CI – Confidence Interval

CV – Cross-Validation

DNA – Deoxyribonucleic Acid

ITS – Internal Transcribed Spacer

IQR – Interquartile Range

LOBO – Leave-One-Banana-Out

LOWESS – Locally Weighted Scatterplot Smoothing

MAE – Mean Absolute Error

MGV – Mean Grey Values

N (obs.) – Number of Observations

OD – Optical Density

OLS – Ordinary Least Squares

PCR – Polymerase Chain Reaction

poly2 – Elastic Net

PMI – Post-Mortem Interval

p-value – Significance of the slope estimate

R^2 – Coefficient of Determination

RH – Relative Humidity

rRNA – Ribosomal Ribonucleic Acid

RMSE – Root Mean Squared Error

ROI - Region of Interest

RPM – Revolutions Per Minute

SD – Standard Deviation

T – Temperature

ΔOD/100 h – Change in Optical Density per 100 hours

1. Introduction

1.1 Forensic application of microbial markers for accurate Post-Mortem Interval estimation

The utilisation of microorganisms as chronological markers has been emphasised in the domain of forensic science as a viable alternative for estimating the post-mortem interval (PMI), particularly in scenarios where conventional methods, such as those based on cadaveric signs (*rigor mortis*, *livor mortis*, *algor mortis*), entomological activity, body cooling rate, or biochemical changes in bodily fluids, are not applicable or present limitations (Amendt et al., 2011; Mathur et al., 2011). Several studies have shown that the process of microbial development and growth during decomposition can be predicted with enough accuracy to allow the development of chronological models that are relevant to forensic science, including for estimating the PMI (Finley et al., 2015; Metcalf et al., 2013). Emerging research also suggests that microbial growth patterns may provide additional temporal insights in forensic contexts (Andrade, 2024).

While most studies in forensic microbiology focus on the analysis of human tissues and soil, recent perspectives have expanded this scope through the field of forensic microbial chronometry, which investigates alternative substrates for temporal estimation (Robinson et al., 2021). Common household food items such as bananas and soup are highly perishable and particularly sensitive to environmental conditions, traits that promote rapid microbial colonisation. These substrates therefore serve as valuable experimental models for observing microbial community dynamics and their potential forensic application. By tracking microbial growth on decomposing food items, investigators can establish a relationship between time since exposure and the degree of decomposition. This approach is particularly pertinent because it broadens the scope of forensic evidence by incorporating traces that would otherwise be disposed of (Hawksworth et al., 2015).

1.2 Gaps in the literature and rationale of the study

Despite the fact that certain studies have evidenced the significance of microbial growth and colonisation in the context of cadaveric decomposition (Finley et al., 2015; Metcalf et al., 2013), there remains a conspicuous paucity of systematic investigations that examine the phenomenon of microbial colonisation and growth in food remains. These substrates, which

are frequently present in domestic environments and often overlooked in traditional forensic analyses, represent an untapped opportunity to broaden the forensic evidence base available at a crime scene.

Moreover, while the extant literature predominantly employs metagenomic techniques (Nam et al., 2023; Pechal et al., 2014), this research proposes a complementary and accessible approach based on classical culture and morphological observation, integrating molecular techniques such as polymerase chain reaction (PCR) and sequencing to confirm species identification. This strategy enables a rigorous and replicable analysis even in laboratories with limited technical resources, thus promoting the forensic applicability of the proposed methodology.

1.3 Forensic microbiology as a complementary tool

Determining the time interval between an event and its discovery is one of the most challenging tasks in reconstructing facts during forensic investigations (Carter et al., 2007). Conventionally, the estimation of the PMI has been based on classical methods, including the analysis of cadaveric changes (*rigor mortis, livor mortis* and *algor mortis*), the presence of necrophagous insects (forensic entomology) and the assessment of the environmental conditions of the site (Henssge et al., 2004). The efficacy of these methods is significantly constrained within closed environments, where environmental factors are more strictly regulated and the presence of external vectors can be mitigated or even eliminated (Amendt et al., 2011).

In this context, the field of forensic microbiology has emerged as a complementary and promising area of research (Hawksworth et al., 2011). Fungal communities exhibit a predictable response, resulting from predictable ecological shifts during decomposition, offer valuable indicators in scenarios where traditional forensic methods are limited in precision or applicability (Eisenhofer et al., 2019). Microbial communities exhibit a predictable response to physico-chemical changes in decomposing substrates, which allows the correlation between colonisation stage and the time since death or exposure (Pechal et al., 2014).

Furthermore, the application of molecular techniques alongside classical microbiology has enabled more precise identification of microorganisms isolated in culture (Gandra et al.,

2008). The capacity to discern microbial communities with a high degree of resolution, even in the early stages of decomposition, contributes substantially to the development of more robust temporal models based on microbial dynamics. Although not yet widely validated, recent investigations indicate promising potential for such approaches in indoor and domestic settings (Oliveira et al., 2023). This approach presents significant advantages in indoor environments and domestic crime scenes, where other forms of temporal estimation, such as entomological activity, may be absent or uninformative. Preliminary findings highlight that microbial indicators could complement traditional PMI estimation methods, particularly in settings lacking conventional evidence (Weçoski et al., 2023).

Consequently, the study of microbial decomposition extends beyond the biological characterisation of decomposing substrates, assuming a pivotal role in forensic investigation (Hawksworth et al., 2015). It provides data that can facilitate the chronology of events, substantiate testimonies, and delineate critical time windows in investigations of disappearances or neglect of the incapable. Its forensic applicability therefore reinforces the role of microbiology as a modern investigative ally, and its increasing acceptance within the field of forensic science is indicative of two interrelated developments (Guo et al., 2023; Robinson et al., 2021). Firstly, it highlights the advancement of scientific and technological capabilities in this domain, and secondly it is a response to the need for methodologies that are more suited to the contemporary reality of crime scenes, which often occur in domestic, enclosed and intricate contexts.

1.4 Food as forensic evidence

In forensic contexts, particularly in domestic environments, the analysis of food remains can provide significant temporal information, offering an ideal substrate for the growth of fungal communities, particularly fungi, whose colonisation dynamics can be exploited as a chronological marker (Nodari et al., 2024). Their presence at crime scenes, cases of disappearance, or investigations into neglect of incapacitated individuals can provide valuable temporal clues about the events in question and add relevant information to expert analysis.

In the context of a crime scene in an enclosed space, for instance, foodstuffs left on a kitchen worktop or dining table may be the sole biological indicators subject to decomposition. The

analysis of fungal colonization on these substrates, or even the observation of visible signs of deterioration, can provide elements to estimate the time that has passed since the last occurrence of human activity at the site. In cases of child neglect or abandonment of the elderly, the decay of prepared but uneaten food can serve as an indicator of the duration of the victim's absence. The significance of these elements is further compounded when integrated with other pertinent evidence, including the degree of environmental organisation, indications of struggle or disorder, and congruence with communications data or electronic surveillance.

Moreover, food, by its very nature, is an organic compound that is rich in nutrients, highly perishable, and susceptible to fungal colonisation. Food decomposition is largely driven by microbial activity and often follows a relatively predictable course under given conditions. Factors such as temperature, ventilation, light exposure, and humidity strongly influence this process, as they directly regulate microbial metabolic activity and the rate at which degradation progresses. Under relatively stable or known environmental conditions, the state of decomposition may therefore serve as a chronological marker (Carter et al., 2007). Also, the presence of such characteristics as high humidity, relatively low pH (bananas pH 4.5–5.2; soups pH 6.0–7.0) the presence of sugars and other bioactive compounds creates a favorable environment for the growth of a variety of microorganisms (Alegbeleye et al., 2022). Growth, succession and identification of these microorganisms can also give very valuable information about the time elapsed between abandonment and discovery.

Despite their potential usefulness, decomposing food is frequently overlooked in criminal investigations and rarely evaluated as chronological traces. This oversight can be ascribed to the absence of standardised protocols for their forensic analysis, as well as the paucity of systematic studies that have documented the pattern of microbial colonisation in common foods as a function of time. However, recent research has demonstrated that certain fungal groups emerge at specific phases of the decomposition process, thereby suggesting that these organisms can function as true chronological markers (Hawksworth et al., 2015).

Given the ubiquity of food in domestic contexts, its systematic study represents a promising avenue for advancing forensic science. The use of substrates such as bananas and soup, which are commonly found in households, offers an experimental model that is representative of

everyday reality. This model allows the observation of microbial colonisation patterns in conditions that simulate real forensic situations, such as bodies discovered in advanced decomposition in private residences, where food remnants are present and may provide additional temporal information. The proposal to analyse these biological traces as temporal markers contributes to the development of applicable microbial chronograms, with the potential to complement and reinforce traditional methods for estimating the temporal interval. The research presented here aims to explore an often neglected forensic resource and to provide a solid empirical basis for the chronological reconstruction of events in domestic environments.

1.5 The role of environmental conditions and substrates

The development of fungal communities over time in organic substrates is dynamic processes that are highly sensitive to environmental conditions. It is widely accepted that temperature and humidity are the primary factors that regulate the rate and pattern of fungal development, thereby directly influencing the rate of food decomposition (Carter et al., 2010; Finley et al., 2015). In domestic environments, where these parameters tend to be more stable than outdoors, fungal growth is more predictable. This situation lends itself to the application of temporal models based on mycological analysis.

Temperature is a pivotal factor, exerting a significant influence on various biological processes such as microbial metabolism, fungal spore germination (Pitt et al., 2009). Specific temperature ranges favour the growth of certain species, while others can be inhibited or even eliminated. This is consistent with experimental evidence showing that when temperatures diverge from the species optimal range, microbial growth is markedly inhibited and can be entirely prevented due to enzyme denaturation and loss of cell membrane function (Nedwell, 2006). Psychrophilic microbes flourish near 0–15°C, mesophiles thrive between 20°C and 45°C, and extremes outside these limits inhibit or eliminate microbial activity (García-Descalzo et al., 2022).

Furthermore, relative humidity (RH) exerts a significant influence on the availability of water in substrates, a factor that is imperative for the survival and metabolic activity of microorganisms (Campos, 2018). Free water is necessary for the absorption of nutrients and for the process of decomposition of food tissues, such as the action of hydrolytic enzymes

produced by fungi and bacteria, which degrade macromolecules present in food, such as starches, proteins, and lipids. Filamentous fungi, such as *P. citrinum* and *Aspergillus spp*., for instance, are capable of producing enzymes including amylases, proteases and lipases. These enzymes facilitate the breakdown of complex structures into smaller molecules, thereby rendering them available for microbial metabolism and accelerating the decomposition process (Pitt et al., 2009). In environments where humidity is controlled, such as the interior of buildings, the greater stability of free water allows these enzymatic processes to occur more linearly and predictably. This facilitates the monitoring of microbial growth and the modelling of microbial successions, thereby strengthening the robustness of temporal estimates (Hawksworth et al., 2015).

In addition to these factors, the pH of the food substrate exerts a substantial influence on fungal composition and growth The presence of certain acid-tolerant fungal groups, such as species of the genera *Penicillium spp, Cladosporium spp* and *Aspergillus spp*, has been observed in association with the decomposition of fruits and other foods with low pH (Martins, 2022). This phenomenon is facilitated by foods with an acidic pH, such as fruits, which create conditions conducive to the growth of these organisms. Conversely, substrates with a more neutral or alkaline pH have been observed to be colonised by diverse fungal species (Rousk et al., 2009). The chemical composition of foods, including sugars, proteins and phenolic compounds, also modulates microbial diversity and decomposition rates.

The interaction of these environmental factors gives rise to specific patterns of fungal growth, which can be monitored to establish an approximate chronology of decomposition and create reliable temporal models that can be utilised in forensic contexts to estimate the time interval elapsed from the state of food decomposition.

1.6. Justification for the choice of food substrates: banana and soup

The selection of food substrates for forensic analysis must take into account two factors. Firstly, the representativeness of the food in real contexts. Secondly, its susceptibility to microbial colonisation. In this study, bananas and soup were selected as the subjects of investigation due to their complementary characteristics, which render them suitable for the study of fungal colonisation dynamics**.**

In Portugal, bananas are widely consumed and are considered to be one of the most common tropical fruits in people's daily diets. As demonstrated in the following data, obtained from FAOSTAT, the average consumption per capita reached 17.9 kg per inhabitant in 2021, a figure that reflects its high availability and acceptance in Portuguese households (Helgi Library, 2021). In addition to their calorific value, bananas are notable for their vitamins, minerals, antioxidants and prebiotic compounds. These characteristics, when considered in conjunction with their climacteric nature and rapid post-harvest deterioration, render them an ideal substrate for microbial colonisation studies of forensic interest.

Conversely, soup can be defined as a staple food commonly found in many households. Its preparation typically involves the use of perishable ingredients, including vegetables, legumes, meat, and broth. The substrate is characterised by its complexity, richness in nutrients, and high water activity. Its composition is influenced by the specific recipe employed and regional dietary habits. The liquid or semi-liquid structure of the substance in question has been shown to facilitate the rapid diffusion of microorganisms and accelerate degradation, particularly when stored at ambient temperature. The selection of soup, therefore, enables the simulation of a realistic domestic scenario and the assessment of fungal growth dynamics in conditions that reflect everyday life in a more comprehensive manner.

Together, these two substrates enable the comparison of microbial colonisation in contrasting matrices—solid and liquid—thus providing a comprehensive view of their forensic potential.

1.7 Limitations of morphological identification and the use of molecular methods

Classical microbiology has traditionally relied on morphological criteria to characterise some fungal communities. However, this approach has significant limitations in forensic science, where a high degree of reliability and accuracy is crucial. Filamentous fungi, for instance, can present similar structures across different genera, which makes it difficult to distinguish between species on the basis of colonial and microscopic morphology alone. This phenotypic similarity renders identification dependent on the analyst's experience and subject to interpretative errors, especially when dealing with environments where multiple microorganisms cohabit and interact with the substrate.

In this context, the integration of molecular methods, such as PCR and the sequencing of specific genetic regions, allows for more rigorous and reproducible identification. These

techniques enable the direct detection of genetic material from cultivated colonies, thereby providing objective confirmation of taxonomic identity. The employment of universal primers for regions such as the Internal Transcribed Spacer (ITS) in the case of fungi, has been demonstrated to be highly effective in distinguishing morphologically similar species, thereby contributing to the validation of potential chronological markers (Ben-Dov et al., 2006; Schoch et al., 2012; White et al., 1990).

In addition to enhancing taxonomic reliability, molecular methods facilitate the comparison of isolates obtained with public genetic databases such as GenBank, thereby promoting the reproducibility of results and facilitating comparisons between different studies. This approach is of particular relevance when attempting to validate models based on fungal growth patterns, as it ensures that the organisms identified are consistent over time and in different experimental contexts.

The objective of this research is to address the above-mentioned knowledge gaps by studying fungal colonisation in common food substrates, specifically bananas and soup, under primarily uncontrolled environmental conditions, with some bananas subsequently analysed under controlled laboratory conditions for validation.

The primary objectives are as follows:

- To identify the predominant fungal species colonising the selected substrates over time.
- To evaluate the influence of environmental factors, such as temperature and humidity, on the speed and pattern of colonisation.
- To analyse the process of banana ripening and integrate its results as a temporal marker.
- To establish temporal patterns of fungal growth that can be used as chronological markers.
- To contribute with experimental data to the development of forensic models that can be applied to the estimation of time intervals within domestic contexts.

The present thesis proposes an accessible, replicable and scientifically based approach to contribute to the consolidation of forensic microbiology as a complementary tool in

reconstructing the chronology of criminal events, opening up space for new investigative applications in indoor environments.

2. Methodology

2.1 Characterisation of the study and definition of the substrate

The research under discussion was conceptualised as an experimental study to identify potential microbial chronological markers present in food substrates commonly encountered in domestic environments (Weçoski et al., 2023). The food substrates selected for analysis were bananas (of the Del Monte brand, originating in Costa Rica) and carrot soup (Continente brand; ingredients: water, potato, carrot 25%, onion, turnip, leek 4%, extra virgin olive oil, salt, garlic; may contain traces of celery, egg, gluten, sulfites, and fish). Each soup used in the assays was purchased as a new batch, introducing natural variability between samples, which represents a limitation of the study. These foods were chosen because they are consumed and discarded at high frequency within households, and also due to the microbial diversity that characteristically colonises them.

The experiments were conducted in a variety of indoor environments — kitchen, bathroom, and living room — as well as in temperature-controlled chambers, to assess the impact of differing environmental conditions, namely temperature (T) and RH, on the development of fungal communities. Each assay was identified by a unique combination of environment and day (assay ID), which was used as the grouping unit in the statistical analyses. An Elitech RC-4HC datalogger (±0.3 °C accuracy, ±3 % RH) was used to monitor environmental conditions, recording measurements every 20 minutes and positioned at the same height as the substrate surface, which facilitated the analysis of temporal patterns of microbial growth.

The methodological sequence followed in this study is summarised in figure 1, which schematically illustrates the main stages of the experimental process that will be described in detail later.

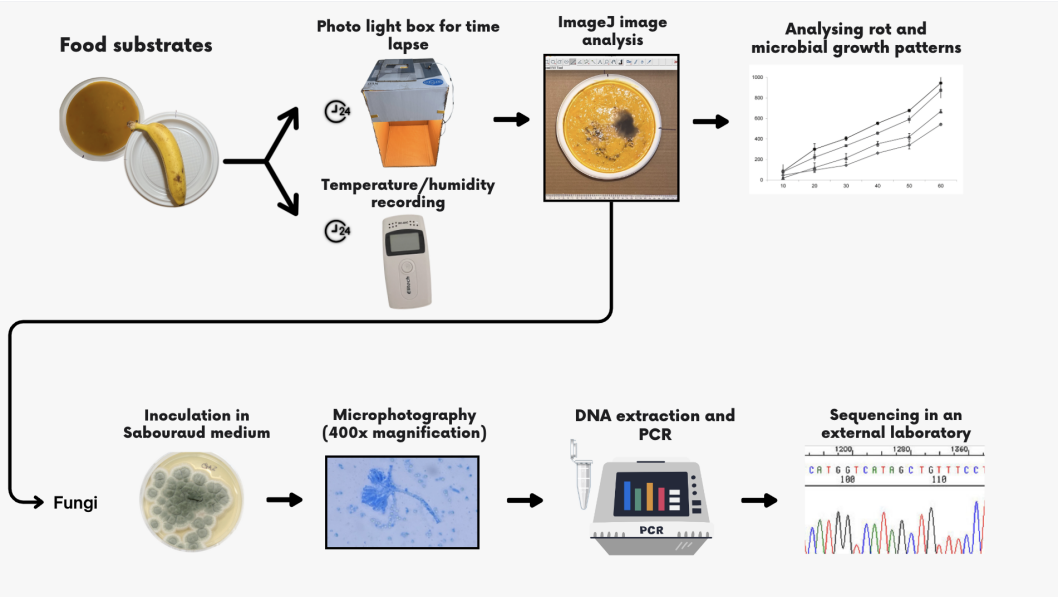

Figure 1 Schematic representation of the experimental workflow, from the assessment of food substrates through environmental monitoring, image analysis, fungal identification, DNA extraction, PCR, and final sequencing in an external laboratory. Figure created by the author using Canva.

2.2 Image acquisition, standardisation, and analysis

The samples were photographed daily in a photographic light box measuring 42 × 44 × 67 cm, to which a 20-centimetre ruler with a matte white reference patch was attached for scale and colour balance control. The images were captured using a digital camera integrated into an iPhone 13 Pro smartphone. The camera was positioned vertically above the samples at a fixed distance of 28 cm, with auto-exposure and auto white balance locked to ensure consistent lighting conditions across all images.

To guarantee constant lighting conditions, an LED bulb, E27 base, 3000 K, 68 W (nominal) was positioned 15 cm above the samples at an approximate 45° angle. Sample T was monitored using the datalogger and did not increase as a result of illumination.

The images obtained throughout the experiment were analysed using specialised ImageJ software, which is widely used for image processing and quantitative analysis in microbiology (Schneider et al., 2012). Utilising this programme, it was possible to measure the growth and development rate of the fungal colonies, establishing parameters such as colony area and diameter at different time intervals. ImageJ facilitates precise measurements,

including the extraction of colour data, and enables the construction of growth curves from digital images captured throughout the experiment.

In the case of bananas, the peel was utilised as an ancillary chronological marker, capitalising on the chromatic transition from yellow to black as a visual indicator of the stage of ripening and decomposition. Consequently, the variation in peel colour was meticulously documented and correlated with the onset and progression of microbial growth. The combination of image analysis and controlled-temperature assays allowed more precise modelling of temporal dynamics.

2.3 Analysis of banana ripening and decomposition

The ImageJ software was utilised to analyse the ripening and decomposition process of bananas over time, employing a standardised protocol to ensure consistency and reproducibility of measurements. The images were converted to greyscale (8-bit) using the Image → Type → 8-bit function, to standardise the intensity of the tones and facilitate quantification. The scale calibration was performed on the basis of a 20-centimetre ruler positioned on the images, thus enabling pixels to be converted to millimetres within the software's measurement environment. After calibration, the pixel size corresponded to 0.12 mm/pixel, based on the reference scale (10.0 mm = 84 pixels). Area measurements were reported to two decimal places (mm^2), consistent with the calibration precision (mm/pixel) and expected error in Region of Interest (ROI) delineation. Colony area and equivalent diameter were then extracted using the (Analyze → Set Scale) and (Analyze → Measure commands).

The analysis of colouration was approached by means of a methodology that entailed the measurement of the mean grey value. This approach was adopted for both the banana peel and a constant white reference area in the image.

The ROI corresponding to the banana peel was delineated with the Freehand Selection tool and stored in the ROI Manager. This ROI was then applied in a standardised manner to all images. Similarly, a ROI was defined over the white reference area. For each image, the mean grey value of the peel and the white area was subsequently measured. The same side of each banana was photographed throughout the experiment, and the ROI was applied consistently across all images. White balance was adjusted manually at the beginning of each

session; however, the absence of a grey reference card is acknowledged as a limitation. Measurements from controlled-temperature assays provided additional robustness in the correlation between OD and time, reducing temperature-related variability.

To standardise the procedure and enable the quantification of the variation in peel colouration over time, the following expression was employed to calculate the Optical Density (OD) based on the Mean Grey Values (MGV**)** of the peel and the white reference area:

$$OD = log10(MGV\ (white)\ /\ MGV\ (banana))$$

The observed OD ranged from –0.044 to 0.731 (see Table 2). OD values were normalised to a constant white reference to ensure comparability across images and timepoints. All OD, T (°C), and RH (%) measurements per banana were extracted and used for modelling. Time prediction from OD followed the same validation framework as the colony-area models (Section 2.10). Features included OD and contemporaneous T and RH, averaged up to each time point to prevent look-ahead bias. Predictive performance was assessed using GroupKFold cross-validation (CV) (K = 5), with banana ID as the grouping factor, ensuring that repeated measurements from the same fruit never appeared simultaneously in training and test folds.

LOWESS (locally weighted scatterplot smoothing) is a non-parametric method that fits simple local regressions to small neighbourhoods of the time axis, weighting observations by proximity (typically with a tricube kernel) and—when desired—iteratively down-weighting outliers. Unlike a global linear or exponential model, LOWESS imposes no fixed functional form on OD(t), allowing the data to reveal non-linearities and phase changes. This is advantageous for ripening because optical density often evolves in stages (slow start, rapid increase, plateau/slowdown) that are poorly summarised by a single global slope. By differentiating the smoothed curve, we obtain an instantaneous rate (ΔOD per hour), which quantifies the typical rate of change (median), identifies peak ripening bursts and their timing, and contrasts early-phase behaviour with later dynamics. LOWESS also tolerates irregular sampling intervals and is comparatively robust to noise, making it well-suited to longitudinal image-derived OD series

The concomitant use of visual markers, such as changes in banana peel colouration, and quantitative data obtained using ImageJ, enabled the development of robust decomposition

models with potential applicability in the identification of relevant temporal markers for forensic purposes.

We evaluated predictive models for time (hours) as a function of OD, mean T, and mean RH per banana. OD was derived from ImageJ MGV, normalised to a white reference (dimensionless). Mean T and RH were computed per banana from the supplied dataset; no external data were used.

Model families compared

1. Linear (inverse) models. Ordinary least squares (OLS) with a flexible feature set to capture curvature and environment interactions:

$$t \sim OD + OD^2 + T + RH + (OD \times T) + (OD \times RH).$$

A Ridge (L2-penalised) variant was also fitted to probe stability against mild regularisation.

2. Tree ensembles. Random Forest and Gradient Boosting regressors were trained on the same feature set to test non-parametric baselines.

3. Mechanistic (two-stage) models. For each banana, we first fitted OD–time curves using either a logistic or Hill function by non-linear least squares, then regressed the resulting curve parameters against the banana's mean T and RH (with log-transforms where appropriate). Predicted parameters for a left-out banana were then used to invert the curve and compute t given (OD, T, RH).

4. Accelerated failure-time (AFT) log-normal models (threshold approach). For each banana, we obtained the LOWESS-smoothed OD(t) trajectory (frac = 0.35) and the crossing times to OD = 0.40 and OD = 0.50 by linear interpolation; only bananas that reached a given threshold were included. We then fitted log(t) to T and RH by OLS (equivalent to a log-normal AFT model), and evaluated predictions by leave-one-banana-out.

5.Validation and statistical evaluation.

Predictive performance was quantified using three complementary metrics: mean absolute error (MAE), root mean squared error (RMSE), and the coefficient of determination (R^2) on held-out folds. For each prediction $\hat{t}_i$ and observed time t_i, we computed:

$$\mathrm{MAE} = \frac{1}{n}\sum\_i = 1^n |t_i - \hat{t}_i|; \quad \mathrm{RMSE} = \sqrt{\frac{1}{n}\sum\_i = 1^n (t_i - \hat{t}_i)^2}; \quad R^2 = 1 - \frac{\sum (t_i - \hat{t}_i)^2}{\sum (t_i - \bar{t})^2}$$

- For linear and ensemble models, metrics were averaged across 5-fold GroupKFold CV partitions, with folds defined by banana ID. This ensured that repeated measurements from the same fruit never appeared simultaneously in training and test sets.
- For mechanistic (logistic/Hill) and AFT models, leave-one-banana-out (LOBO) validation was applied: the OD–time trajectory of each banana was excluded in turn, parameters were estimated from the remaining bananas, and predictions made for the excluded fruit.

To reduce sensitivity to fold allocation, GroupKFold partitions were repeated with different random seeds and the distribution of errors pooled. For LOBO, each banana yielded one test prediction, and metrics were computed across the 13 hold-outs.

For internal robustness checks, bootstrap resampling at the banana level (B = 400 replicates) was also performed on the OLS model. This provided empirical distributions of MAE, RMSE, and R^2, from which 95% confidence intervals (percentiles 2.5–97.5) were extracted. All preprocessing (standardisation, polynomial feature generation, interaction terms) was carried out within each training fold only, ensuring strict separation between training and test data.

2.4 Measurement of microbial colony areas

The quantification of microbial growth on food substrates was conducted by measuring the area of each colony individually using ImageJ software. The images were previously calibrated based on the 20-centimetre ruler included in the field of view, converting pixel values to millimetres.

The visible colonies were delineated individually with the Freehand Selection tool, with due consideration for the morphological contours of each structure. Following the selection process, the ROI were added to the ROI Manager (Analyze → Tools → ROI Manager), thus enabling their management and sequential measurement.

The measurements were performed using the (Analyze → Measure) function, after the initial configuration of the system using the (Set Measurements) option. At this stage, the 'Area' parameter was selected as the primary metric. Measurements of colony area were reported to two decimal places to reflect the effective precision of the calibration (0.12 ± 0.01 mm/pixel).

The areas of all colonies were measured individually in each image, corresponding to the different days of analysis. The data obtained enabled the construction of microbial growth curves over time, allowing a quantitative assessment of colonisation dynamics as a function of the environmental conditions recorded. For a subset of assays conducted under controlled-temperature conditions, the uncertainty associated with temperature effects was reduced, contributing to increased robustness of the subsequent predictive modelling. This approach provided a solid foundation for the application of predictive microbiology models and for the identification of potential microbial chronological markers with relevance in forensic contexts.

In addition to the measurement of colony area, a manual count of clearly visible and well-defined colonies presents in the frontal plane of each acquired image was performed. This quantification applied exclusion criteria for aggregations, overlapping colonies, or out-of-focus regions, allowing only individualizable units to be counted.

2.5 Inoculation, isolation and morphological characterisation of microorganisms

Food samples exhibiting overt indications of microbial colonisation were analysed using an Optika SZX-TA stereoscopic microscope (OPTIKA Microscopes, Italy), which facilitated magnifications of up to x400, thereby enabling meticulous observation of colonial morphology. In light of the observations made, regions which exhibited a variety of microorganisms were selected for further investigation. A representative colony of each microorganism was selected for individual inoculation in the appropriate culture media. Colonies were collected at early stages of visible growth, only when they were clearly distinguishable and spatially separated on the substrate; whenever overlapping growth was

observed, or when one colony appeared to develop over another, these areas were excluded from collection to avoid mixed microbial material. Each isolate was assumed to represent a single species; therefore, when identification was only possible at the genus level, isolates were designated as *genus sp*., rather than *genus spp*. Concurrently, continuous monitoring of microbial development was conducted directly on the food substrate, with collections being made at various stages of colonisation. For colonies that were subcultured (replicated) onto fresh media, colony area measurements were not continued, as the primary focus was on monitoring growth dynamics on the original food substrate. Subcultured plates were instead used for species identification purposes: portions of the colonies were examined microscopically to observe hyphal and spore morphology, and additional material was used for deoxyribonucleic acid (DNA) extraction and molecular identification. The methodology employed in this study enabled the monitoring of temporal changes in dominant fungal presence by assessing the maintenance or replacement of the initially dominant microorganism. This phenomenon is characteristic of environments in which intermicrobial competition occurs. Consequently, the ability to trace the isolated strains at various stages of growth was ensured, thereby minimising the risks of cross-contamination between different cultures and preserving representative samples for subsequent analysis.

For the isolation of filamentous fungi and yeasts, Sabouraud culture medium with chloramphenicol (Batch 4020062, Manufacturer Biolife) was utilised, to inhibit bacterial growth. The samples were initially suspended in sterile peptone water (Batch 165214, Manufacturer Scharlau), ensuring adequate homogenisation of the microbial suspension.

When deemed necessary, serial dilutions were performed in sterile peptone water (10^{-1} to 10^{-6}) to obtain suspensions with adequate microbial concentration for the isolation of individual and pure colonies. This procedure was deemed particularly relevant for samples exhibiting high microbial load or where multiple species were observed to be growing in conjunction.

All inoculations were performed in a Class II laminar flow cabinet disinfected with 70% ethanol (contact time ≥ 5 min) and UV irradiation (15 min) to ensure aseptic conditions. Fungal cultures were plated using the spread method, with each isolate plated in triplicate. Plates were incubated at 25 °C in the dark for 5–7 days under ambient RH (not controlled),

and cultures were monitored daily for colonial development. Sterile medium plates were included as negative controls in each session to assess potential contamination and ensure experimental quality.

Following the incubation period and the development of colonies in the culture media, a detailed macroscopic analysis of the morphological characteristics was performed, using a stereoscopic magnifying glass whenever necessary. The following aspects were evaluated: shape (circular, irregular or filamentous); size; colour (both on the surface and on the reverse side of the colony); edge characteristics (smooth, wavy or lobed); and surface texture (smooth, rough, shiny or opaque). The observations were meticulously documented through the medium of photographs, thus contributing to the formation of a systematic image bank of the cultures in question.

The characterisation of the fungal isolates was conducted through the utilisation of images obtained by optical microscope analysis at a magnification of x400. The preparation of slides utilised lactophenol blue as a mounting medium and dye, thereby facilitating detailed visualisation of morphological structures pertinent to taxonomic identification, including hyphae, sporangia, conidia and conidiophores. In instances where practicable, identification was undertaken in accordance with conventional taxonomic keys, incorporating considerations of morphological characteristics (Ellis, 2007; Walsh et al., 2018). The combination of conventional microbial characterisation techniques, encompassing macroscopic and microscopic analysis, facilitated an initial categorisation of the isolates. This procedure was fundamental for the subsequent stages of identification and analysis.

2.6 DNA extraction and purification for molecular analysis

Genomic DNA extraction from fungal cultures was performed based on the modified protocol of (Ferreira et al., 2000), as adapted by the Mycology and Microbiology Research Group (MMRG), with specific changes for this study. Fungal colonies were transferred to Eppendorf tubes and subjected to cell lysis with a buffer composed of 0.5% (w/v) SDS, 0.24 M NaCl, 0.26 M Tris-HCl and 0.025 M EDTA. The solution was supplemented with 1% 2-mercaptoethanol (v/v).

The mixture was incubated at 65 °C for one hour, vortexing every 20 minutes to promote cell lysis. Subsequently, extraction was performed with a mixture of phenol:chloroform: isoamyl

alcohol (25:24:1, v/v/v). The recovered aqueous phase was subjected to precipitation with isopropanol. The pellets obtained were washed with 70% ethanol, air-dried and resuspended in ultrapure, sterile water. The concentration and purity of the extracted DNA were assessed by spectrophotometry using NanoVue™ equipment (GE Healthcare). Subsequently, the samples were diluted according to the requirements for PCR amplification.

2.7 PCR amplification and visualisation

Amplification of the ITS region of fungal DNA was performed by PCR, using the primers ITS1 (5'-TCCGTAGGTGAACCTGCGG-3') and ITS4 (5'-TCCTCCGCTTATTGATATGC-3'), recommended for molecular identification of fungi due to their high capacity for species discrimination (White et al., 1990). These primers allow the amplification of a fragment between 300 and 900 bp in size, comprising the ITS1 regions, the 5.8S rDNA gene and ITS2. When amplification with the ITS1/ITS4 primer pair was not obtained**,** it was necessary to use alternative combinations of primers, such as ITS1 and ITS2 (5'-GCTGCGTTCTTCATCGATGC-3') or ITS3 (5'-GCATCGATGAAGAACGCAGC-3') and ITS4, to obtain adequate amplification. PCR reactions were performed using 35 cycles, with specific thermal profiles for each primer pair: for ITS1/ITS2, 95 °C for 30 s, 53 °C for 30 s, and 72 °C for 30 s, followed by a final extension at 72 °C for 10 min; for ITS3/ITS4, 95 °C for 30 s, 56 °C for 30 s, and 72 °C for 45 s, followed by a final extension at 72 °C for 7 min; and for ITS1/ITS4, 95 °C for 30 s, 53 °C for 30 s, and 72 °C for 1.5 min, followed by a final extension at 72 °C for 10 min. The reactions were prepared with GoTaq® DNA Polymerase (Ref M7808, Promega).

The entire volume of each PCR reaction was loaded onto the agarose gel for electrophoretic analysis. The amplified products were visualised by electrophoresis in 2% agarose gel, using agarose for electrophoretic separation of nucleic acids (Lot. 23D054120, GeneON GmbH Bioscience), stained with GreenSafe Premium (NZYTech®). To estimate the size of the amplified fragments, an appropriate molecular weight marker (HyperLadder™ 100 bp, Bioline) was used. Bands were analysed under UV light, and the quality of amplification was confirmed by the presence of a single band of expected size.

2.8 Extraction and purification of DNA fragments from agarose gel

The bands corresponding to the amplified fragments were visualised under ultraviolet light on a transilluminator and subsequently excised with the aid of a sterile scalpel. Each sample was transferred to an Eppendorf container.

Purification was performed in accordance with an internal protocol based on thermal lysis of agarose with a dissolution buffer containing guanidine thiocyanate (GuSCN 5.5 M), Tris-HCl 100 mM (pH 6.6) and EDTA 10 mM (pH 8.0). This procedure promotes protein denaturation and facilitates DNA binding to silica. The samples were incubated until the agarose was completely dissolved. After adding isopropanol, which increases the affinity of DNA for the silica matrix, the mixture was transferred to silica columns and centrifuged. The eluate was discarded, and the columns were washed with PE Buffer (10 mM Tris-HCl, pH 7.5, with 80% ethanol). Subsequently, impurities were removed and, finally, DNA was eluted from the columns with heated ultrapure water. The purified DNA was stored at -20 °C or sent for sequencing.

2.9 Confirmation of molecular identification

The samples were dispatched to StabVida (Caparica, Portugal) for sequencing, which was carried out using Sanger sequencing technology. The analysis was conducted using specific primers for the ITS region (ITS1, ITS2, ITS3, and ITS4) as required for each sample. The results were made available in the form of .seq and .ab1 (chromatograms) files, which were viewed using the SnapGene Viewer application (GSL Biotech LLC). The sequences obtained were then compared with data available in the NCBI GenBank public database using the BLAST (Basic Local Alignment Search Tool) tool to validate the identification of microorganisms previously characterised by morphological analysis (Altschul et al., 1990). Sequence acceptance required ≥99% identity and alignment length ≥500 bp (see Annex Table 1A). The actual sequence lengths (in bp) are now explicitly listed in the annex to confirm compliance. In cases where a few sequences were shorter, the threshold was adapted to ≥99% identity and ≥90% query coverage, with justification provided. The top-hit species for each sequence was recorded along with its GenBank accession number, and sequences were only considered confirmed if they met this identity criterion.

2.10 Time prediction from colony area

Time (hours) was modelled as a function of colony area (mm^2) and the per-assay mean T (°C) and RH (%) for each species separately. Species-specific mean T and RH values were computed per assay and merged to all time points. As this may introduce *information leakage*, we included (or propose to include) a sensitivity test comparing (a) per-assay means and (b) time-varying environmental averages up to each time point (t). This allows quantifying any potential bias introduced by the simplification. When such testing is not performed, the possible overestimation of accuracy should be explicitly acknowledged. We compared four model families: (i) polynomial ridge regression (area, environment, and all two-way interactions; degree 2), (ii) elastic net (degree-2 polynomial), (iii) gradient boosting, and (iv) random forest. We selected these four complementary model families for their ability to capture nonlinear effects and environmental interactions in small samples. First, penalised polynomial regressions (ridge and elastic net, degree 2) were chosen to provide interpretable baselines, allowing us to capture potential non-linear effects of colony area and its interactions with T and RH, while controlling for collinearity and overfitting. These models are appropriate given the relatively small sample size per species and the repeated-measures design. Hyperparameters were tuned via nested CV, exploring α and l1_ratio grids for ridge and elastic net regressions; *n_estimators*, *max_depth* and *min_samples_leaf* for random forest; and *n_estimators*, *learning_rate* and *max_depth* for gradient boosting.

Second, we included two non-linear ensemble learners—gradient boosting and random forests—because they can flexibly model complex relationships, accommodate heterogeneity between assays, and remain robust in the presence of noise. Random forests offer stability through bagging and variance reduction, whereas gradient boosting sequentially improves predictive accuracy by focusing on residual error.

We did not extend the comparison to deep learning or more complex time-series architectures because (i) the number of observations per species is modest and does not warrant models with very high parameterisation, (ii) the predictor set is low-dimensional (colony area, T, RH), and (iii) transparency and ease of interpretation are critical in forensic contexts. The chosen families thus provide a balance of statistical rigour, interpretability, and predictive flexibility, matched to the size and structure of the dataset.

To avoid leakage across repeated measures from the same assay, performance was estimated with GroupKFold CV (K = 5) using the assay ID (Soup/Banana) as the grouping factor. This ensured that repeated measurements from the same assay never appeared simultaneously in training and test sets. This ensured that predictions were validated on unseen assays, simulating a realistic forensic application. We report MAE hours, RMSE hours, and R^2. Hyperparameters for the penalised linear models were selected by internal CV; tree models used default, conservative settings.

The best-performing model family was then trained on the full spp dataset using colony area, per-assay mean T, and per-assay mean RH as predictors. To provide uncertainty bands suitable for casework, we fitted quantile gradient boosting models ($\alpha = 0.10, 0.50, 0.90$) and report PI10–PI90, corresponding to the 10th–90th percentiles of the predicted time distribution, as an empirical 80% prediction interval around the point estimate. Coverage of the 80% interval was verified on held-out validation folds to ensure reliability for casework applications. This reflects indoor conditions captured by the present dataset.

3. Results

3.1 Quantitative Analysis of Banana Ripening

Figure 2 summarises the ripening trajectories OD for all bananas over time; curves are colour-coded and annotated with each banana's mean T and RH, showing faster increases under warmer/drier conditions and slower under cooler/more humid settings

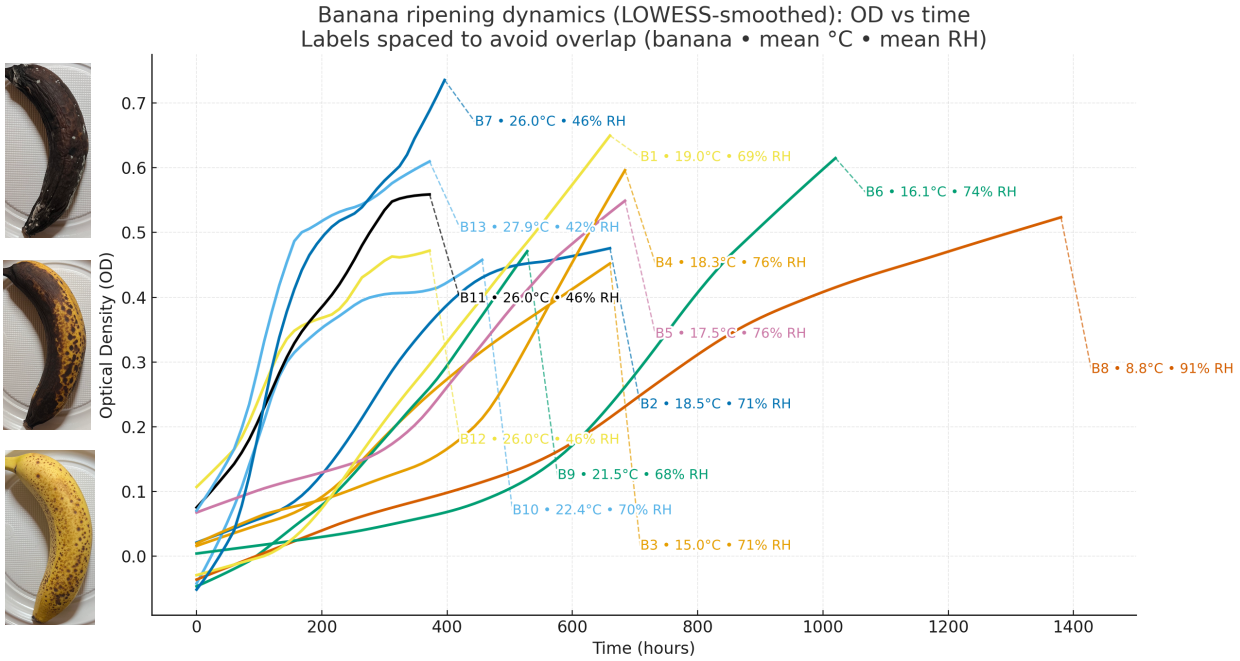

Figure 2. Dynamics of banana ripening (OD vs time, LOWESS-smoothed) across 13 bananas. The images on the left illustrate the typical visual stages observed during ripening, ranging from early yellow, to ripe, to over-ripe/blackened fruit. OD - Optical density.

Each coloured line is a LOWESS-smoothed trajectory (frac = 0.35) of OD over time (hours). Labels placed near the line ends report the banana ID, followed by mean T (°C) and mean RH (%); dashed connectors are used only to avoid label overlap. OD was derived from ImageJ mean grey values normalised to a white reference (dimensionless); higher OD reflects a darker/browner appearance. Raw data points are omitted for clarity. Study periods varied considerably between bananas (n=13), ranging from 372 to 1380 hours (median: 660 hours). These differences reflect the fact that individual colonies reached stable optical density levels at different times and under variable T and RH conditions. The shortest observation periods were for bananas 7, 11, 12, and 13 (372-396 hours), whilst banana 8 had the longest observation period (1380 hours). Initial OD values ranged from -0.040 to 0.106, with most

bananas beginning in an unripe state. Final OD values ranged from 0.452 to 0.731 (median: 0.543), indicating successful ripening progression across all specimens. The total change in OD ranged from 0.371 to 0.761 units (median: 0.534), with banana 7 showing the most substantial change and banana 12 the least. Ripening rates varied from 0.0004 to 0.0019 OD units per hour (median: 0.001). Substantial variation was observed both within and between bananas. For the region of the banana surface that was selected for analysis, T ranges associated with individual bananas varied considerably. Some bananas were maintained under controlled temperature (e.g. 26.0–26.0 °C for bananas 7, 11 and 12), while others experienced ambient indoor conditions, showing considerable fluctuations (e.g. 3.2–12.8 °C for banana 8 and 20.1–33.6 °C for banana 13). RH showed extensive variation, with individual banana ranges spanning from narrow control (44.0-48.4% for bananas 7, 11, 12) to broad variation (30.0-60.9% for banana 13, 84.2-95.9% for banana 8).

Table 1 summarises the overall ripening dynamics across all bananas studied. Initial OD values were slightly negative or close to zero (−0.040 to 0.106), reflecting the calibration to the white reference.

Table 1. Ripening Dynamics Summary

Metric	Range	Median
Initial Optical Density	-0.040 - 0.106	-0.011
Final Optical Density	0.452 - 0.731	0.543
Total OD Change	0.371 - 0.761	0.534
Average Rate (OD/hour)	0.0004 - 0.0019	0.0010
Study Duration (hours)	372 - 1380	660

Final values reached between 0.452 and 0.731, yielding total OD changes of 0.371–0.761 with a median of 0.534. The average rate of increase was modest, ranging from 0.0004 to 0.0019 OD per hour, with a median of 0.0010. Study durations varied from 372 to 1380 hours, capturing both early-terminating and extended observation periods.

Across the 13 bananas, the series comprised 32–116 observations and spanned 0–372 h (Bananas 11–13) to 0–1380 h (Banana 8). OD ranges, reflecting the banana ripening dynamics, were broadly similar, with upper bounds typically 0.45–0.69 and the highest maximum in Banana 7 (0.731); lower bounds were near zero or slightly negative due to white

normalisation. Environmental conditions varied widely: a cool, very humid profile (Banana 8: mean 8.8 °C; RH 90.8%) contrasted with warmer–drier settings (Bananas 7, 11–12: fixed 26.0 °C; RH ≈46%; Banana 13: 27.9 °C on average, RH 42.1%). Most remaining series ran at ~15–22 °C with RH ~69–76%. In sum, Table 2 documents broad environmental contrast alongside comparable OD amplitudes across bananas.

Table 2. Descriptive summary by banana (n=13)

Banana	n (obs.)	Observation period (h)	OD range	Temperature mean ± SD (°C)	Temperature range (°C)	Relative humidity, mean ± SD (%)	Relative humidity range (%)
1	56	0–660	-0.031–0.635	19.0 ± 1.4	16.5–21.5	68.6 ± 8.2	56–82
2	56	0–660	-0.006–0.496	18.5 ± 1.4	16.0–21.5	70.8 ± 7.3	53–81
3	56	0–660	-0.011–0.452	15.0 ± 2.3	11.3–19.5	71.1 ± 9.0	52–85
4	58	0–684	0.009–0.568	18.3 ± 0.8	16.6–20.3	75.6 ± 7.8	61–86
5	58	0–684	0.032–0.543	17.5 ± 0.5	16.5–18.2	76.1 ± 7.2	60–87
6	86	0–1020	-0.028–0.598	16.1 ± 1.2	13.3–18.4	74.1 ± 10.2	50–87
7	35	0–396	-0.030–0.731	26.0 ± 0.0	26.0–26.0	45.9 ± 1.3	44–48
8	116	0–1380	-0.041–0.531	8.8 ± 2.7	3.2–12.8	90.8 ± 1.9	84–96
9	45	0–528	-0.044–0.536	21.5 ± 0.4	21.0–22.7	68.3 ± 6.5	56–79
10	39	0–456	-0.025–0.477	22.4 ± 0.8	21.2–23.6	70.5 ± 7.2	56–80
11	32	0–372	0.083–0.591	26.0 ± 0.0	26.0–26.0	46.0 ± 1.3	44–48
12	32	0–372	0.106–0.685	26.0 ± 0.0	26.0–26.0	46.0 ± 1.3	44–48
13	32	0–372	0.073–0.607	27.9 ± 3.4	20.1–33.6	42.1 ± 9.3	30–61

Optical density (OD) is computed from ImageJ mean grey values normalised to a white reference. Temperatures (°C) and relative humidity (%) correspond to the recorded ambient conditions.

Slopes (ΔOD per 100 h) were uniformly positive and highly significant (all $p < 1\times10^{-12}$), indicating consistent increases in OD over time (see Table 3).

Table 3. Linear slopes of OD per banana estimated with ordinary least squares (OLS). Slopes expressed as ΔOD per 100 hours with 95% confidence intervals; R^2 from the linear fit.

Banana	Linear slope (ΔOD / 100 h)	95% CI (ΔOD / 100 h)	R^2	p-value (slope)
1	0.111	0.107 to 0.116	0.979	7e-47
2	0.085	0.079 to 0.091	0.934	1.42e-33
3	0.073	0.071 to 0.076	0.983	3.13e-49
4	0.074	0.066 to 0.083	0.844	2.84e-24
5	0.076	0.070 to 0.081	0.927	1.62e-33
6	0.062	0.057 to 0.067	0.875	1.05e-39
7	0.198	0.175 to 0.221	0.904	7.95e-18
8	0.046	0.045 to 0.048	0.96	1.22e-81
9	0.099	0.094 to 0.105	0.972	2.28e-34
10	0.099	0.081 to 0.117	0.78	1.03e-13
11	0.149	0.139 to 0.159	0.966	1.3e-23
12	0.115	0.095 to 0.134	0.829	4.91e-13
13	0.149	0.122 to 0.177	0.804	3.77e-12

Abbreviations: OLS – ordinary least squares; OD – optical density (ImageJ mean grey value normalised to white reference); ΔOD/100 h – change in optical density per 100 hours (linear slope); CI – confidence interval; R^2 – coefficient of determination; *p*-value – significance of the slope estimate.

Rates varied by roughly fourfold (0.046–0.198), with the slowest progression in Banana 8 (0.046; cool, very humid profile) and the fastest in Banana 7 (0.198; warmer, drier), while Bananas 11 and 13 also showed high rates (0.149). Bananas 1, 9 and 10 sat in an intermediate band (≈0.099–0.111), and Bananas 2–6 clustered at lower-to-mid values (≈0.062–0.085). Model fit was strong across series (R^2 = 0.78–0.983), supporting an approximately linear trajectory within the observed windows; tighter confidence intervals in extensively sampled series (e.g., Bananas 1, 3, 8) contrast with wider intervals where sampling was briefer (e.g., Bananas 10, 12, 13). In practical terms, a slope of 0.10 corresponds to ~0.001 OD per hour (~0.024 per day), so Banana 7 ripening progresses at about twice this rate (~0.048 per day), whereas Banana 8 ripening advances at roughly half (~0.011 per day). Overall, the pattern is consistent with faster ripening under warmer/drier conditions and slower under cooler/more humid settings; unadjusted associations to be corroborated by stratified or adjusted analyses.

In short, Table 4 complements the OLS results (Table 3) by mapping when ripening accelerates most and how strongly, rather than only how much on average.

Table 4. LOWESS-based rate summaries per banana.

Banana	n (obs.)	Median LOWESS rate (ΔOD / 100 h)	Peak LOWESS rate (ΔOD / 100 h)	Time at peak rate (h)	Early-phase median rate (ΔOD / 100 h)
1	56	0.121	0.14	246.0	0.028
2	56	0.048	0.155	282.0	0.037
3	56	0.066	0.102	270.0	0.033
4	58	0.044	0.182	570.0	0.04
5	58	0.076	0.123	390.0	0.034
6	86	0.05	0.13	750.0	0.013
7	34	0.163	0.482	102.0	0.175
8	116	0.037	0.071	690.0	0.038
9	44	0.106	0.139	426.0	0.049
10	39	0.068	0.309	114.0	0.234
11	32	0.135	0.22	114.0	0.117
12	32	0.094	0.235	102.0	0.099
13	32	0.074	0.416	102.0	0.17

Median and peak rates are computed from the first derivative of the LOWESS-smoothed OD curve; times are expressed in hours from the start of observation. Abbreviations: LOWESS – locally weighted scatterplot smoothing; OD – optical density (ImageJ mean grey value normalised to white reference); ΔOD/100 h – change in optical density per 100 hours; n (obs.) – number of observations.

LOWESS-derived rates were positive but heterogeneous. Median rates spanned 0.037–0.163 ΔOD/100 h, with the slowest in Banana 8 (0.037) and the fastest in Banana 7 (0.163). Peak rates varied widely (0.071–0.482 ΔOD/100 h), revealing two timing archetypes: an early-peaking cluster (Bananas 7, 10–13) with high peaks at ~102–114 h (0.220–0.482) and elevated early-phase medians (0.099–0.234), and a late-peaking cluster (Bananas 1–6, 8–9) with more moderate peaks (0.102–0.182) occurring later (246–750 h). For most bananas, early-phase rates were below the overall median, indicating acceleration after the first quartile; in the early-peaking cluster, the opposite pattern suggests an initial surge followed by deceleration (e.g., Banana 10: early 0.234 vs median 0.068). As a guide, 0.10 per 100 h ≈ 0.024 OD/day; thus, Banana 7 advances ≈0.039/day, whereas Banana 8 advances ≈0.009/day. Overall, Table 4 indicates non-linear ripening kinetics with environment-sensitive timing, complementing linear slopes by localising when ripening bursts occur.

To explore the effect of T on ripening dynamics, the banana samples were stratified into tertiles (stratum) according to their mean T. Table 5 summarises the resulting groups and their corresponding OD patterns.

Table 5. Stratified descriptive summaries by temperature tertiles (based on banana-level mean temperature).

Stratum	Bananas (n)	Observations (n)	Observation period (h)	OD mean ± SD	OD median [IQR]	OD range	Linear slope (ΔOD / 100 h)
High T	**4**	130	0–396	0.378 ± 0.193	0.427 [0.198–0.536]	-0.030–0.731	0.155
Mid T	**4**	195	0–660	0.248 ± 0.186	0.276 [0.059–0.413]	-0.044–0.635	0.094
Low T	**5**	374	0–1380	0.227 ± 0.178	0.166 [0.075–0.384]	-0.041–0.722	0.046

Abbreviations: T – mean temperature; OD – optical density (ImageJ mean grey value normalised to white reference); SD – standard deviation; IQR – interquartile range; ΔOD/100 h – change in optical density per 100 hours (linear slope).

Stratifying by tertiles of banana-level mean T revealed a clear monotonic gradient in ripening intensity. The High-T stratum showed the highest central tendency (OD mean ± SD 0.378 ± 0.193; median [IQR] 0.427 [0.198–0.536]) and the steepest linear progression (ΔOD/100 h = 0.155), the Mid-T stratum was intermediate (0.248 ± 0.186; 0.276 [0.059–0.413]; 0.094), and the Low-T stratum the lowest (0.227 ± 0.178; 0.166 [0.075–0.384]; 0.046). Although OD ranges overlapped (upper bounds up to ~0.72–0.73 across strata), the shift in medians and slopes indicates faster ripening at warmer temperatures. Observation windows differed (High-T 0–396 h; Low-T up to 0–1380 h), yet the longest follow-up coincided with the smallest slope, reinforcing that the gradient is not explained by time-window alone.

To complement the temperature-based summaries, ripening patterns were also examined across tertiles (stratum) of mean RH. Table 6 presents the corresponding descriptive indicators for each humidity group.

Table 6 Stratified descriptive summaries by relative humidity tertiles (based on banana-level mean RH).

Stratum	Bananas (n)	Observations (n)	Observation period (h)	OD mean ± SD	OD median [IQR]	OD range	Linear slope (ΔOD / 100 h)
High RH	**4**	318	0–1380	0.229 ± 0.184	0.159 [0.076–0.400]	-0.041–0.722	0.046
Mid RH	**4**	207	0–660	0.258 ± 0.178	0.290 [0.071–0.412]	-0.031–0.635	0.084
Low RH	**5**	174	0–516	0.323 ± 0.207	0.357 [0.139–0.514]	-0.044–0.731	0.109

Abbreviations: RH – relative humidity; OD – optical density (ImageJ mean grey value normalised to white reference); SD – standard deviation; IQR – interquartile range; ΔOD/100 h – change in optical density per 100 hours (linear slope).

An inverse gradient was observed across humidity tertiles. Low-RH exhibited the highest central tendency (OD mean ± SD 0.323 ± 0.207; median 0.357 [0.139–0.514]) and the steepest slope (ΔOD/100 h = 0.109), Mid-RH was intermediate (0.258 ± 0.178; 0.290 [0.071–0.412]; 0.084), and High-RH the lowest (0.229 ± 0.184; 0.159 [0.076–0.400]; 0.046). OD ranges again overlapped (maxima ~0.72–0.73), implying that high end-values can occur across strata, but typical levels and rates shift towards faster ripening under drier conditions. Notably, the High-RH stratum had the broadest observation window (0–1380 h) yet the slowest slope, which, together with the temperature results, supports a pattern where warmer and drier environments are associated with quicker OD increases. These summaries remain descriptive and should be interpreted alongside adjusted analyses to account for co-variation between temperature and humidity.

To evaluate and compare the predictive accuracy of different modelling approaches for estimating time from OD, mean T, and mean RH, Table 7 summarises the performance metrics (MAE, RMSE, R^2) for each model under the corresponding CV protocol.

Table 7. Predicting time (hours) from OD, mean temperature (°C), and mean relative humidity (%)

Best	Model family	CV protocol	MAE (h)	RMSE (h)	R^2
★	Linear OLS (with OD², interactions)	5-fold GroupKFold (by banana)	91.1	109.3	0.756
	Ridge (linear, penalised)	5-fold GroupKFold (by banana)	91.2	109.5	0.756
	Random Forest	5-fold GroupKFold (by banana)	127.1	161.4	0.560
	Gradient Boosting	5-fold GroupKFold (by banana)	127.8	153.9	0.617
	Logistic-time (params ~ T, RH)	Leave-one-banana-out (LOBO)	209.7	465.5	−1.518
	Hill-time (params ~ T, RH)	Leave-one-banana-out (LOBO)	175.1	258.8	0.222
	AFT log-normal (time to OD = 0.40)	Leave-one-banana-out (LOBO)	110.3	172.1	0.491
	AFT log-normal (time to OD = 0.50)	Leave-one-banana-out (LOBO)	200.3	419.1	−0.367

Abbreviations: OD – optical density (ImageJ mean grey value normalised to white reference); OLS – ordinary least squares; CV – cross-validation; MAE – mean absolute error; RMSE – root mean squared error; R^2 coefficient of determination; GroupKFold – cross-validation grouped by banana identity; LOBO – leave-one-banana-out validation; AFT – accelerated failure time.

The linear OLS model with OD^2 and interaction terms achieved the best out-of-sample accuracy (MAE 91.1 h; RMSE 109.3 h; $R^2 = 0.756$), with Ridge essentially identical (MAE 91.2 h; RMSE 109.5 h; $R^2 = 0.756$). Non-parametric tree ensembles were clearly weaker (Random Forest: MAE 127.1 h; $R^2 = 0.560$; Gradient Boosting: MAE 127.8 h; $R^2 = 0.617$). Two-stage mechanistic approaches generalised poorly under LOBO (Logistic-time: MAE 209.7 h; $R^2 = -1.518$; Hill-time: MAE 175.1 h; $R^2 = 0.222$). The AFT log-normal threshold models performed moderately at OD = 0.40 (MAE 110.3 h; RMSE 172.1 h; $R^2 = 0.491$), but less well at OD = 0.50 (MAE 200.3 h; RMSE 419.1 h; $R^2 = -0.367$) owing to the smaller effective sample (only bananas that reached 0.50 OD). On these data, a parsimonious linear model of time on OD, T and RH (with OD^2 and interactions) offers the best accuracy and the most stable generalisation. Mechanistic and threshold-based alternatives are informative for interpretation and event-time questions but are not superior to the primary task of predicting time given (OD, T, RH).

The ordinary least squares model with OD^2 and interaction terms showed strong agreement between observed and predicted ripening times, as illustrated in the calibration plot (Figure

3). Most points clustered close to the identity line, indicating a good overall fit, with only a few deviations at extreme values. Examination of residuals against humidity (Figure 4) revealed no systematic bias, supporting the adequacy of the model across the observed environmental range. Finally, the nomogram-style curves (Figure 5) demonstrated the practical predictive use of the model, showing how the estimated ripening time increases with OD under three representative indoor scenarios (18 °C / 70% RH, 22 °C / 50% RH, and 26 °C / 40% RH). These curves highlight the forensic applicability of the model, enabling time estimation from an observed OD measurement when approximate ambient conditions are known.

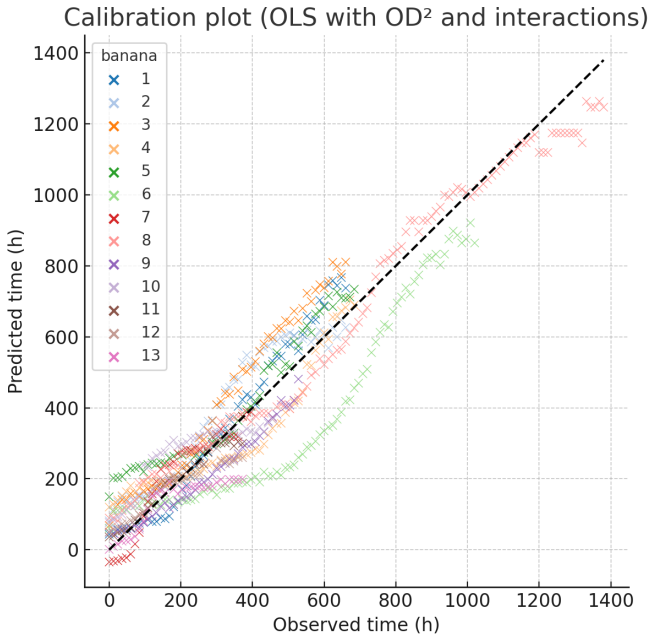

Figure 3. Calibration of the OLS model (OD² + interactions). Scatterplot of predicted versus observed ripening times (hours), coloured by banana ID, with the identity line (dashed). The model shows good overall calibration, with most points clustering near the identity line. OD - Optical density.

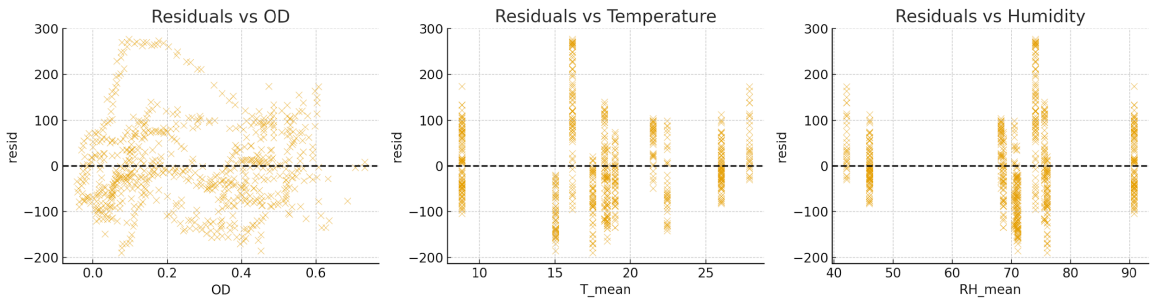

Figure 4. Residual diagnostics for the OLS model. Residuals (observed – predicted, hours) plotted against OD, mean temperature, and mean relative humidity. No strong systematic biases are apparent across predictors, supporting model adequacy. RH - Relative humidity; OD - Optical density.

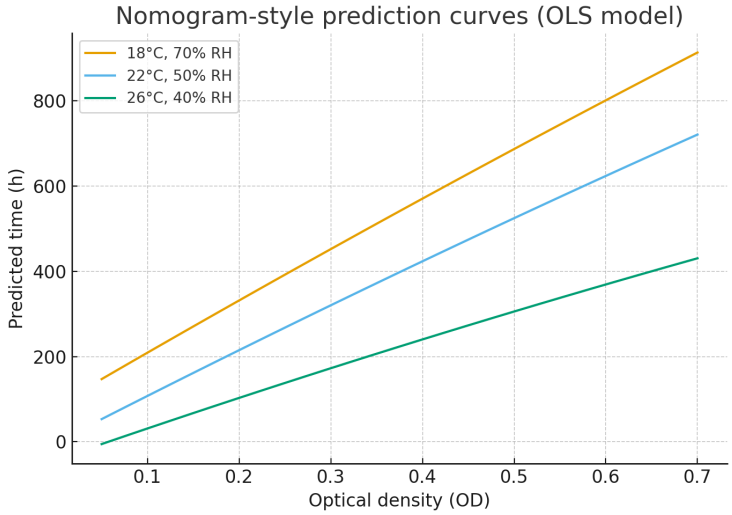

Figure 5. Nomogram-style prediction curves from the OLS model. Predicted ripening time as a function of optical density (OD) under three environmental scenarios (18 °C/70% RH, 22 °C/50% RH, 26 °C/40% RH). The curves provide a forensic tool for estimating elapsed time from observed OD, given average indoor conditions. RH - Relative humidity.

The two-dimensional sensitivity analysis (Figure 6A) confirmed the expected environmental effects: higher mean T shortened the predicted ripening time, whereas higher RH prolonged it. The response surface illustrates that temperature exerts the strongest influence, but humidity modulates the rate substantially under cooler conditions. The companion uncertainty map (Figure 6B) shows the bootstrap-derived 95% prediction interval width across the same grid, with larger uncertainty observed at the extremes of the environmental spectrum. Together, these figures demonstrate that the model not only captures the environmental dependence of ripening dynamics but also quantifies the associated margins of error, providing a transparent basis for forensic time estimation.

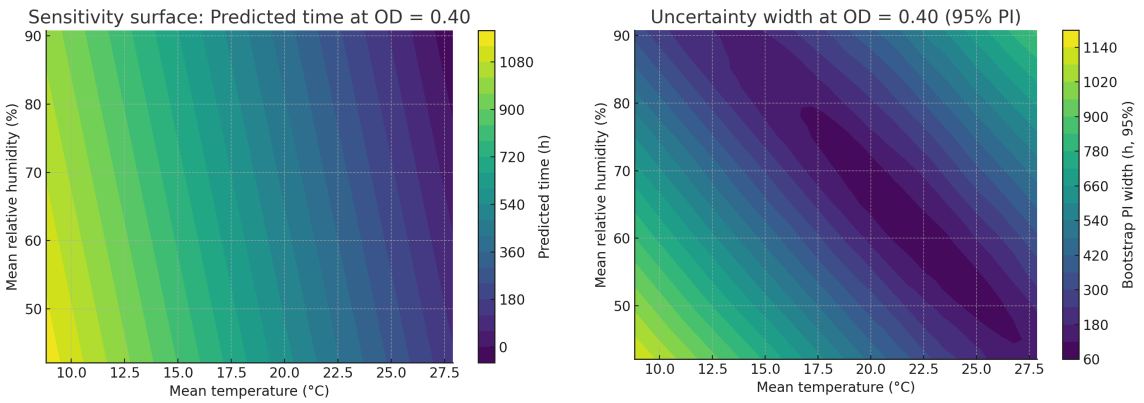

Figure 6. A. Two-dimensional sensitivity surface (OLS model, OD = 0.40). Predicted ripening time (hours) as a function of mean temperature (°C) and relative humidity (%). Higher temperatures accelerate, and higher humidity slows, the estimated time to reach OD = 0.40; B. Prediction uncertainty surface (bootstrap 95% interval width, OD = 0.40). Width of the 95% prediction interval (hours) across the same environmental grid. Greater uncertainty is observed at the extremes of temperature and humidity. PI - Predicted interval; OD - Optical density.

The simulated forensic cases (Table 8) illustrate the practical utility of the OLS model with OD^2 and interaction terms. For a banana with OD = 0.35 under moderate indoor conditions (20 °C, 65% RH), the estimated elapsed time was approximately 323 h, with a 95% prediction interval of ±80 h. Under slightly warmer and drier conditions (22 °C, 50% RH), a higher OD of 0.45 corresponded to an estimated 356 h, with narrower uncertainty (±72 h). Conversely, a lower OD of 0.30 in cooler and more humid conditions (18 °C, 75% RH) produced a longer estimate of 364 h with wider uncertainty (±93 h). These examples confirm that the model provides interpretable predictions with quantified margins of error, directly supporting forensic inference of time since deposition from observed OD and ambient conditions.

Table 8. Forensic case simulations using the OLS model (OD^2 + interactions).

Case	OD	Temp (°C)	RH (%)	Predicted time (h)	95% PI lower (h)	95% PI upper (h)	± Half-width (h)
A	0.35	20.0	65.0	322.7	245.6	405.7	80.1
B	0.45	22.0	50.0	356.0	293.5	436.4	71.5
C	0.30	18.0	75.0	363.8	283.2	468.7	92.7

Predicted ripening times (hours) with bootstrap 95% prediction intervals for three illustrative cases, defined by optical density (OD) at observation and mean indoor conditions (temperature and relative humidity). These examples highlight the model's direct applicability for forensic estimation of elapsed time since deposition. PI - Predicted interval; RH, Relative humidity. Temp – Temperature; OD - Optical density.

All visible microbial development corresponded to fungal colonies, which were subsequently identified morphologically and molecularly. Therefore, the results presented below refer exclusively to fungal dynamics.

3.2 Qualitative results – Banana

Visual monitoring of fungal colonisation in banana samples revealed progressive alterations to the surface. Initially, small white or green spots appeared, which later expanded into visibly distinct fungal growth structures with distinct morphological characteristics (see Figure 7).

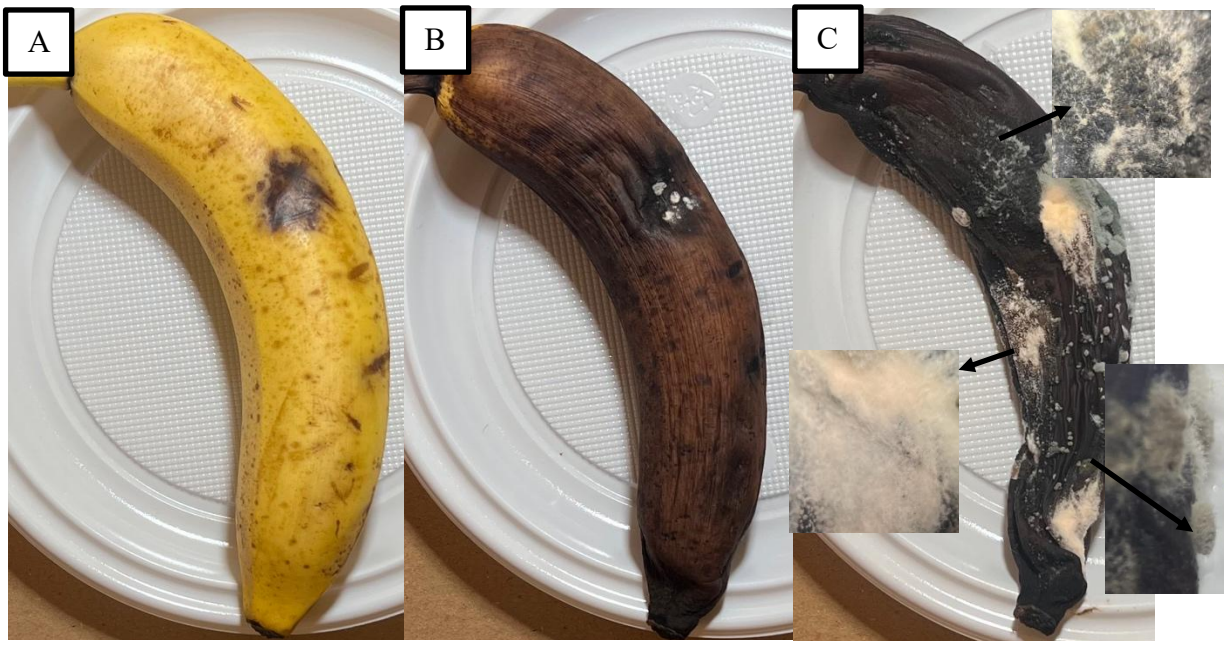

Figure 7. Evolution of fungal colonization in experimental banana samples over time**.** (A) Banana at the time of exposure (time 0); (B) Twenty-nine days after exposure, showing the early stages of surface colonization; (C) Fifty-five days after exposure, with representative colonies highlighted by arrows, corresponding to enlarged images obtained with a magnifying glass (Magnification 40×).

After isolation in culture medium, morphological differences between the species were confirmed (Figure 8). *P. citrinum* maintained its characteristic pigmentation and *M. caribbica* retained its yeast-like creamy growth, *Fusarium verticillioides* (*F. verticillioides*) presented diffuse, cottony colonies with a pinkish reverse, which were distinct from the other isolates.

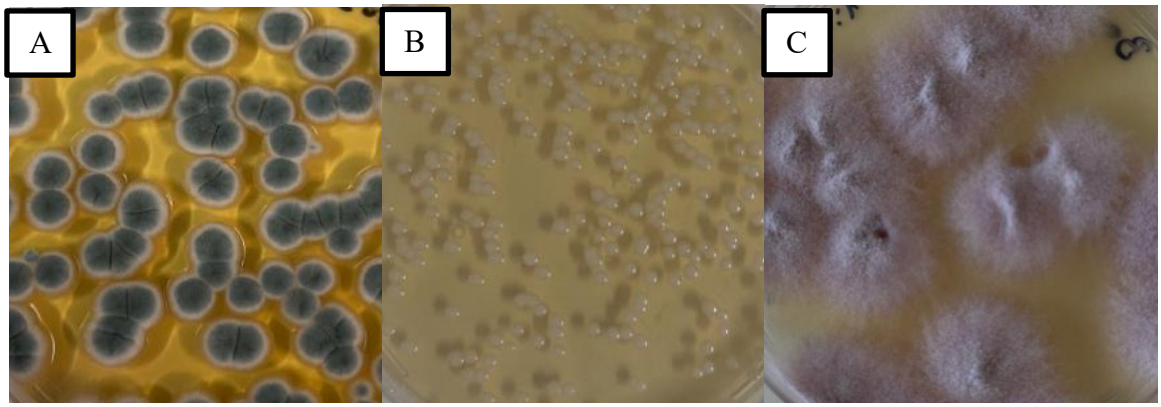

Figure 8. Fungal colonization on Sabouraud Chloramphenicol culture medium. (A) *P. citrinum* showing compact colonies with blue-green pigmentation; (B) *M. caribbica* exhibiting yeast-like, whitish colonies with creamy texture; (C) *Fusarium* sp. producing cottony colonies with white to pink pigmentation. (Magnification 1×; Dilution 1:10,000).

Microscopy revealed diagnostic structures that were confirmed by the sequencing results (see Figure 9 and Annex 1). *P. citrinum* (GenBank accession PV369845) exhibited branched conidiophores with characteristic conidial chains; *M. caribbica* (GenBank accession MG016004) displayed oval yeast cells; and *F. verticillioides* (GenBank accession MN121533) presented sickle-shaped (fusiform) macroconidia. These findings agreed with the taxonomic identifications obtained through molecular sequencing. These images corroborate the molecular data and reinforce the reliability of the identifications.

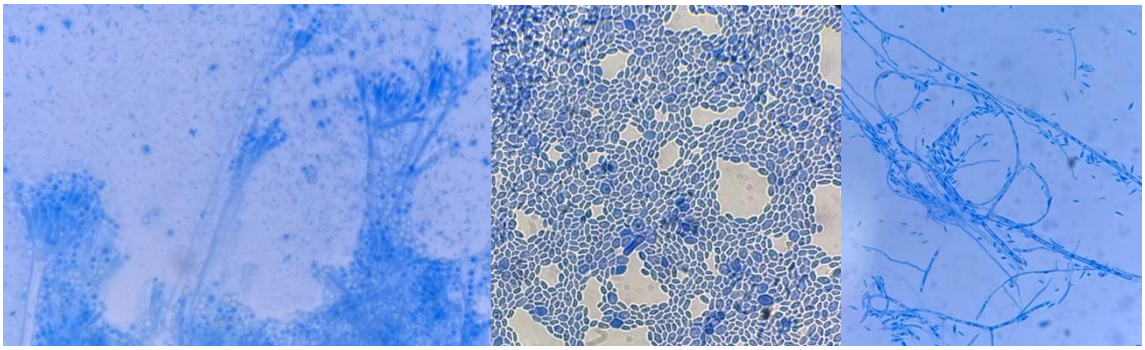

Figure 9. Microscopic structures of fungal colonies stained with lactophenol cotton blue, corresponding to molecular identifications: (A) *P. citrinum*: branched conidiophores with conidia chains; (B) *M. caribbica*: oval yeast cells; (C): *F. verticillioides* fusiform macroconidia (Magnification 400x).

3.3 Quantitative results Banana

The environmental conditions recorded varied significantly among the living room, bathroom, and kitchen settings. The living room exhibited the greatest thermal amplitude,

with mean T around 19 °C, reaching peaks of up to 33.6 °C, and a moderately high RH (~69%) with wide fluctuations (30–86%). The bathroom showed slightly lower mean T (17.5–21.5 °C) and comparable or slightly higher RH levels (68–76%). The kitchen, in turn, presented the lowest mean T (as low as 8.8 °C in some samples) and the highest and most stable RH levels (up to 90.8%, ranging between 84–96%). In addition to these domestic settings, a subset of bananas was maintained under controlled temperature (26 °C) and relative humidity (46%)**.** This allowed comparison of fungal growth under stable conditions with that observed in fluctuating indoor environments.

Three fungal species were consistently detected in the majority of the banana assays that developed fungal growth: *F. verticillioides, M. caribbica, and P. citrinum* (Table 9). Of the 13 bananas assayed, 7 showed fungal growth under experimental conditions with modest variation in mean T (13.7–16.9 °C) and RH (74.1–83.1%), reflecting relatively stable indoor storage environments. No colonies developed on the remaining 6 bananas exposed to higher T (26–30 °C), indicating that fungal growth is inhibited under these conditions.

In the quantitative analysis of fungal colonization on bananas, the number of colony forming units (CFU) per banana was recorded for each species. *P. citrinum* showed counts ranging from 1 to 7 CFU per banana, *F. verticillioides*. ranged from 1 to 4 CFU, and *M. caribbica* displayed lower counts between 1 and 2 CFU. These counts reflect the relative prevalence of each species under the experimental conditions.

Table 9. Descriptive statistics of indoor fungal colony growth on abandoned bananas

Species	No. of observations	No. of bananas	Temperature (°C, mean ± SD)	Humidity (%, mean ± SD)	Colony area (mm², range)	Growth duration (h, range)
F. verticillioides	606	7	13.7 ± 4.7	83.1 ± 10.0	0.0 – 151.2	0 – 3756
M. caribbica	345	6	16.8 ± 1.2	74.1 ± 9.6	0.0 – 6.3	0 – 840
P. citrinum	440	7	16.9 ± 1.5	75.5 ± 6.3	0.0 – 3.2	0 – 1186

F. verticillioides exhibited the broadest temporal window, with colonies monitored for up to 3756 h (~156 days) and attaining the largest colony sizes (up to 151.2 mm²). In contrast, *M. caribbica* and *P. citrinum* displayed markedly restricted growth ranges: maximum colony

areas remained below 7 mm² and 4 mm², respectively, over shorter observation periods (≤1186 h).

These descriptive findings highlight distinct interspecific patterns. *F. verticillioides* demonstrates both sustained growth and wide temporal coverage, suggesting potential robustness for long-term temporal estimation. By contrast, *M. caribbica* and *P. citrinum* appear limited to narrow spatial and temporal niches, which may constrain their forensic utility unless considered as complementary markers within shorter post-exposure intervals.

The growth trajectories of *F. verticillioides*, *M. caribbica* and *P. citrinum* observed on ripe bananas highlighted clear interspecific differences (Figure 10).

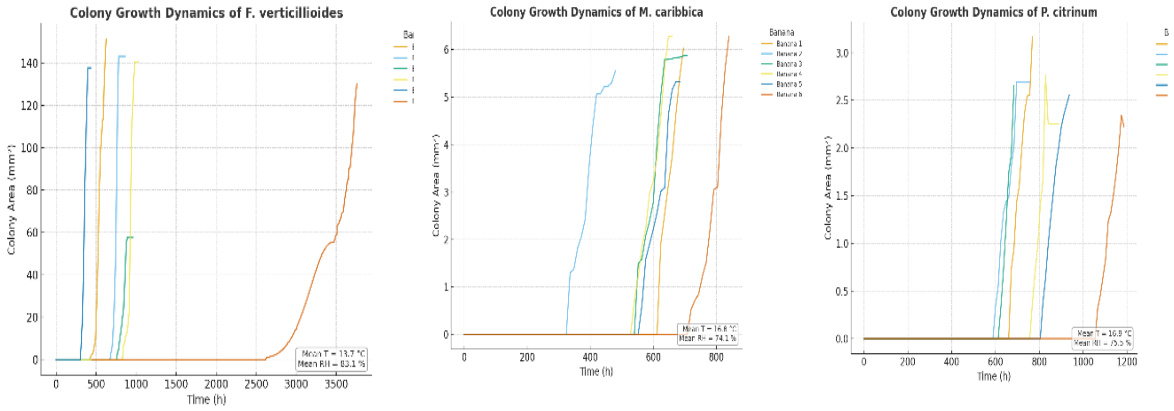

Figure 10. Colony growth dynamics of *F. verticillioides, M. caribbica* and *P. citrinum* in abandoned bananas under indoor conditions. Each line represents a distinct banana assay, showing progressive expansion of colony area (mm²) over time (hours).

F. verticillioides demonstrated fast and prolonged growth, with colonies continuing to expand for more than 150 days under cooler, humid conditions, suggesting strong potential as a long-term temporal marker. By contrast, *M. caribbica* exhibited minimal development, with small colonies and a short detection window, while *P. citrinum* displayed intermediate growth behaviour but remained spatially limited. These trends suggest that, on ripe bananas, *F. verticillioides* offers the most informative temporal signal, whereas *M. caribbica* and *P. citrinum* may serve as supplementary indicators only within restricted time frames.

3.3.1 Bananas – Model Comparison Tables

Table 10 presents the performance of all tested models per species, based on MAE, RMSE, and R^2.

Table 10. Cross-validated model performance per species.

Species	Model	MAE (h)	MAE SD	RMSE (h)	RMSE SD	R^2
F. verticillioides	Linear (Area + Env + Interactions, RidgeCV)	646.6	527.4	777.0	609.3	-4.075
	Elastic Net (poly2)	656.2	535.6	783.4	616.8	-4.106
	Gradient Boosting	531.0	616.0	596.5	677.5	-0.843
	Random Forest	531.8	620.0	597.5	685.1	-0.833
M. caribbica	Linear (Area + Env + Interactions, RidgeCV)	168.1	42.2	195.8	50.7	0.096
	Elastic Net (poly2)	170.4	40.8	197.8	49.3	0.078
	Gradient Boosting	160.6	52.7	195.4	59.6	0.072
	Random Forest	161.0	52.9	195.5	59.9	0.071
P. citrinum	Linear (Area + Env + Interactions, RidgeCV)	213.7	64.6	252.5	78.1	0.095
	Elastic Net (poly2)	211.3	60.8	249.9	72.4	0.111
	Gradient Boosting	196.2	48.3	231.0	54.7	0.239
	Random Forest	195.5	46.1	230.2	53.5	0.242

MAE – mean absolute error; RMSE – root mean squared error; R^2 – coefficient of determination.

Based on the results shown in Table 10, the best model for each species is summarised in Table 11.

Table 11. Best model per species (summary)

Species	Best model	MAE (h)	RMSE (h)	R^2	No. of bananas	No. of observations
F. verticillioides	Gradient Boosting	531.0	596.5	-0.843	7	606
M. caribbica	Gradient Boosting	160.6	195.4	0.072	6	345

P. citrinum	Random Forest	195.5	230.2	0.242	7	440

MAE – mean absolute error; RMSE – root mean squared error; R^2 – coefficient of determination.

For *F. verticillioides*, the Gradient Boosting model achieved an MAE of 531.0 h, RMSE of 596.5 h, and R^2=−0.843 (7 bananas; 606 observations), indicating very poor predictability driven by the extremely wide temporal span of up to 3756 h. *M. caribbica* growth was best captured by Gradient Boosting, with MAE 160.6 h, RMSE 195.4 h, and R^2=0.072 (6 bananas; 345 observations), representing a weak but slightly positive fit. *P. citrinum* performed best with a Random Forest model, yielding MAE 195.5 h, RMSE 230.2 h, and R^2=0.242 (7 bananas; 440 observations), which reflects modest predictive ability and the highest R^2 among the three species.

The extreme temporal range of *F. verticillioides* resulted in very large absolute errors and a negative R^2. Both *M. caribbica* and *P. citrinum* produced only modest signals, with the best R^2 observed at 0.242 (*P. citrinum*, Random Forest), implying considerable residual error for forensic timing. Across species, colony area remained the principal driver of predictions, while environmental factors added only modest incremental value. However, substrate effects and the presence of very long and heterogeneous timelines reduced model learnability.

The relative contributions of colony area, T, and RH varied considerably across species (Table 12).

Table 12. Feature importances in best models per species

Species	Feature	Importance
F. verticillioides	Colony area	0.309
	Mean temp	0.441
	Mean RH	0.250
M. caribbica	Colony area	0.779
	Mean temp	0.166
	Mean RH	0.055
P. citrinum	Colony area	0.695
	Mean temp	0.203
	Mean RH	0.102

Feature importance is expressed as the proportion of variance explained by each predictor in the best-performing model. Mean temp – mean temperature; Mean RH – mean relative humidity.

In *F. verticillioides*, environmental parameters dominated, with mean T (0.441) and RH (0.250) together accounting for more variance than colony area (0.309). This suggests that growth trajectories of *F. verticillioides* on bananas are more sensitive to ambient conditions than to colony size alone.

In contrast, *M. caribbica* and *P. citrinum* displayed greater reliance on colony area, with importances of 0.779 and 0.695, respectively. For these species, T and RH contributed only modestly (≤0.20), indicating that growth expansion itself provides the primary temporal signal, while environment acts as a secondary modifier.

The prediction grids (Table 13) provide practical estimates of elapsed time under species-average conditions.

Table 13. Predicted time (hours) at species-average environment

Species	Colony area (mm²)	Predicted time (h)
F. verticillioides	1	397.2
	5	602.9
	10	635.7
	20	640.7
	30	646.4
M. caribbica	1	588.0
	5	657.7
	10	706.8
	20	706.8
	30	706.8
P. citrinum	1	633.8
	5	719.5
	10	719.5
	20	719.5
	30	719.5

Predicted time (hours) corresponds to species-average indoor environment values. Values are generated from the best model per species. Colony area expressed in mm².

For *F. verticillioides*, predicted times exceeded 600 h once colonies reached ≥5 mm², rising only marginally with further expansion, reflecting saturation of the growth signal**.** *M. caribbica* showed a steep increase from ~588 h at 1 mm² to over 700 h at 10 mm², but values plateaued thereafter, suggesting limited temporal discrimination at later stages. *P. citrinum* similarly produced clustered predictions between 634 h and 720 h across the 1–30 mm² range, again pointing to restricted discriminatory power.

Figure 11 illustrates the predicted elapsed time as a function of colony area and environmental conditions for *P. citrinum*, showing modelled surfaces for (A) T and (B) RH.

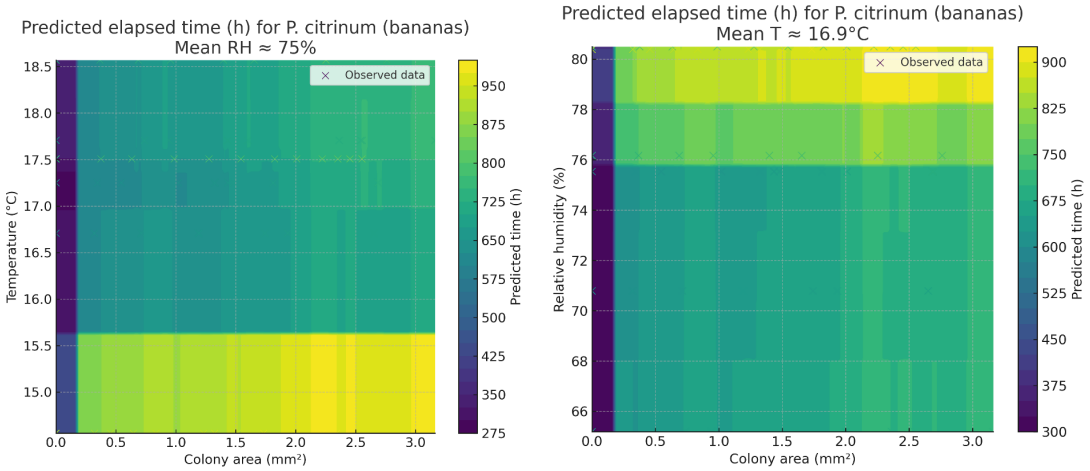

Figure 11. **A.** Predicted elapsed time (h) for *P. citrinum* as a function of colony area and temperature on bananas, at mean relative humidity (≈76%). Contour shading illustrates the joint effect of colony expansion and temperature on temporal estimates. **B.** Predicted elapsed time (h) for *P. citrinum* as a function of colony area and relative humidity on bananas, at mean temperature (≈17 °C). Predictions indicate a minor contribution of relative humidity to modelled elapsed time.

The predictive surface of elapsed time as a function of colony area and T (Figure 11A) shows that colony expansion was the dominant driver of modelled time, with T exerting only a minor modifying effect. Predicted elapsed times rose with increasing colony area, but clustered within a narrow band of ~150–250 h, reflecting limited temporal discrimination. Overlay of observed data confirmed that the model captured the general trajectory but was constrained by a lack of variability in the dataset.

When RH was introduced as the environmental variable (Figure 11B), the surface remained largely flat. RH had negligible influence on predicted elapsed time, and predictions again converged toward a restricted window, regardless of colony size. These results indicate that *P. citrinum* on bananas provided a weak environmental signal, with growth dynamics largely insensitive to modest fluctuations in humidity.

The quantile-based uncertainty analysis (Figure 12) confirmed the narrow predictive range and modest discriminative value. The median curve increased steadily with colony area, but the empirical 80% prediction intervals (PI10–PI90) were wide relative to the narrow median trajectory, often spanning >40 h. This highlights considerable residual uncertainty and

reduces the potential forensic value of *P. citrinum* growth on bananas as a biomarker of elapsed time.

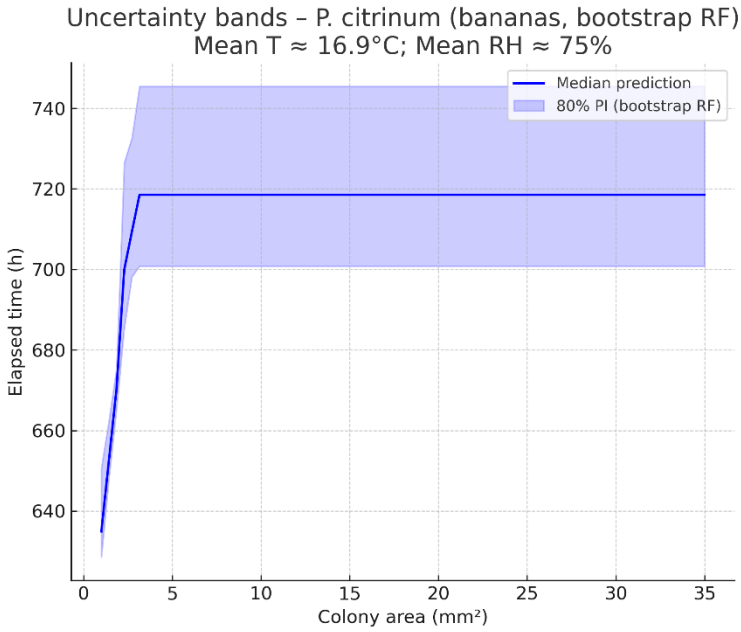

Figure 12. Uncertainty bands for *P. citrinum* predictions derived from quantile gradient boosting models. The central blue line denotes the median prediction, and the shaded region represents the empirical 80% prediction interval (PI10–PI90), at mean indoor conditions (temperature ≈17 °C; RH ≈75%).

3.4 Qualitative results - Soup

In addition to quantitative data, visual observations of the fungal colonization process in the experimental soups were recorded. The images provide representative documentation of the macroscopic and microscopic changes that accompanied the progression of growth. Macroscopic evolution: visible surface changes were observed, initially with small whitish or greenish spots corresponding early fungal growth structures. Over the following days, these growth structures expanded, differing in morphology and pigmentation (Figure 13).

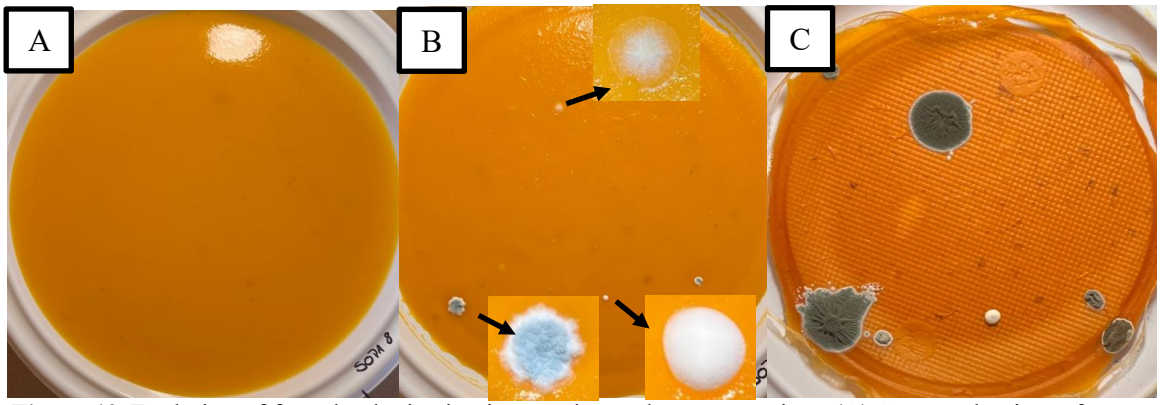

Figure 13. Evolution of fungal colonization in experimental soup over time. (A) Soup at the time of exposure (time 0); (B) Six days after exposure, with three colonies highlighted by arrows, corresponding to the enlarged images obtained with a magnifying glass (Magnification 40x); (C) Sixteen days after exposure, showing the expansion of colonies and morphological differences between species.

Cladosporium cladosporioides (*C. cladosporioides*) was characterized by the development of grayish-green colonies with a velvety appearance and diffuse distribution. *M. caribbica* showed more discreet growth, generally in creamy formations with well-defined boundaries and a smaller surface area. *P. citrinum* formed blue-green colonies that were compact and regular in outline.

Isolation in culture medium: The samples transferred to culture media confirmed the morphological differences between species (Figure 14). While *P. citrinum* (GenBank accession PV369845) maintained its characteristic pigmentation on agar, *C. cladosporioides* (GenBank accession MF476044) developed diffuse colonies with a dark reverse, and *M. caribbica* (GenBank accession MG016004) exhibited yeast-like growth, with a creamy texture and whitish coloration.

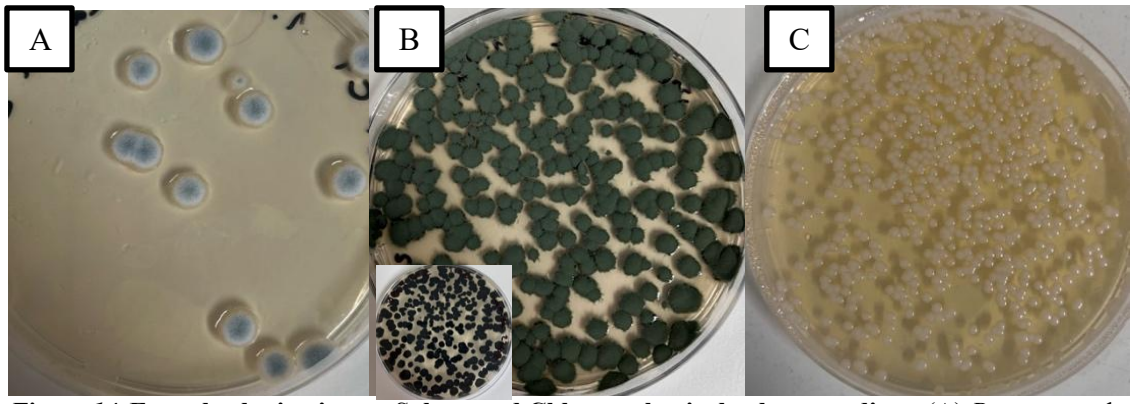

Figure 14. **Fungal colonization on Sabouraud Chloramphenicol culture medium.** (A) *P. citrinum* showing blue-green pigmentation and compact colony; (B) *C. cladosporioides* with diffuse colony and dark reverse (inset in the corner of the image); (C) *M. caribbica* exhibiting yeast-like growth, creamy texture, and whitish coloration. (Magnification 1x; Dilution 1:10,000).

Microscopy Observations under optical microscopy revealed structures confirmed by subsequent molecular identifications. In *P. citrinum*, it was possible to observe branched conidiophores with chains of conidia, while *C. cladosporioides* exhibited conidia in branched chains, and *M. caribbica* showed oval cells typical of yeast (Figure 15 and Annex 1). These images corroborate the molecular sequences obtained and reinforce the reliability of the taxonomic identifications.

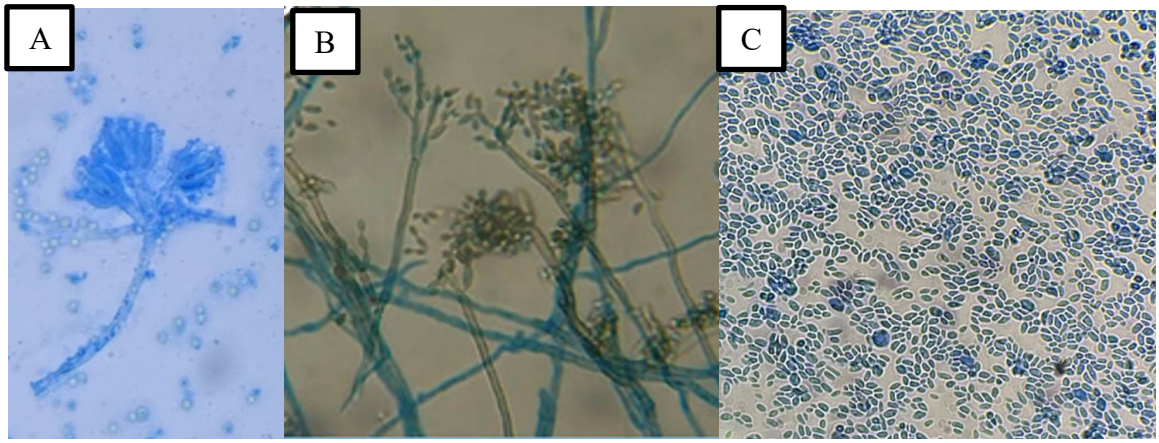

Figure 15. Microscopic structures of fungal colonies stained with lactophenol cotton blue, corresponding to molecular identifications: (A) *P. citrinum*: branched conidiophores with chains of conidia; (B) *C. cladosporioides*: conidia arranged in branched chains; (C) *M. caribbica*: oval-shaped yeast cells (Magnification 400x)

3.5 Quantitative results Soup

The environmental conditions recorded for the soup samples varied only slightly between the kitchen and living room settings. All soup containers developed fungal growth during the observation period. The kitchen exhibited an average T of 20.35 °C and a RH of 71.45%, whereas the living room presented a comparable mean T of 20.45 °C but a slightly lower RH of 68.55%.

Three fungal genera were consistently observed in the soup assays: *C. cladosporioides*, *M. caribbica*, and *P. citrinum*. The CFU counts revealed that *P. citrinum* ranged from 4 to 5 CFU per sample, *C. cladosporioides* from 2 to 4 CFU, and *M. caribbica* from 1 to 2 CFU. These results indicate a greater predominance of *P. citrinum* in the soup substrate, followed by *C. cladosporioides*, while *M. caribbica* appeared as a secondary colonizer with limited but consistent occurrence.

Table 14 presents descriptive statistics of fungal colony growth for three species in soups, including T, relative humidity, colony area, and growth duration.

Table 14. Descriptive statistics of indoor fungal colony growth in abandoned soups

Species	No. of observations	No. of soups	Temperature (°C, mean ± SD)	Humidity (%, mean ± SD)	Colony area (mm², range)	Growth duration (h, range)
C. cladosporioides	108	6	21.7 ± 4.5	70.8 ± 8.7	0.0 – 106.2	0 – 300
M. caribbica	67	3	19.9 ± 4.2	72.8 ± 7.1	0.0 – 28.5	0 – 312
P. citrinum	105	5	23.0 ± 2.5	69.3 ± 8.2	0.0 – 31.6	0 – 264

Across the experimental soups, three fungal species were consistently identified: *C. cladosporioides*, *M. caribbica*, and *P. citrinum*. The experimental conditions showed moderate indoor variability, with mean T ranging from 19.9 °C to 23.0 °C and mean RH between 69.3% and 72.8%. Colony expansion displayed clear interspecific differences: *C. cladosporioides* attained the largest colony areas (up to 106.2 mm²), whereas *M. caribbica*

and *P. citrinum* remained below 30 mm². Growth durations varied by dataset, extending up to 312 h in *M. caribbica* assays, 300 h for *C. cladosporioides*, and 264 h for *P. citrinum*.

Figure 16 illustrates the growth dynamics of *C. cladosporioides*, *M. caribbica*, and *P. citrinum* in soups, showing colony area expansion over time for each assay.

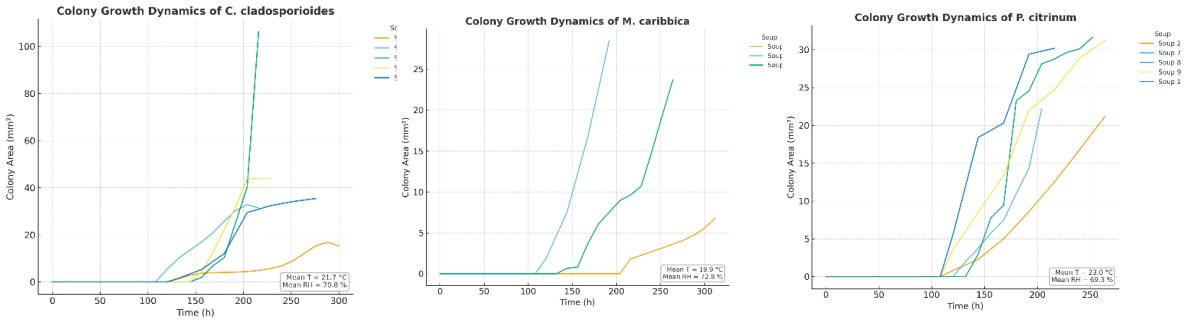

Figure 16. Colony growth dynamics of *C. cladosporioides, M. caribbica* and *P. citrinum* in abandoned soups under indoor conditions. Each line represents a distinct soup assay, showing progressive expansion of colony area (mm²) over time (hours).

3.5.1 Soups –Model Comparison Tables

Table 15 presents the cross-validated performance metrics of all tested models per fungal species, including MAE, RMSE, and R^2.

Table 15. Cross-validated model performance per species

Species	Model	MAE (h)	MAE SD	RMSE (h)	RMSE SD	R^2
C. cladosporioides	Linear (Area + Env + Interactions, RidgeCV)	70.4	32.9	87.4	45.5	-0.878
	Elastic Net (poly2)	68.8	30.5	83.5	39.2	-0.603
	Gradient Boosting	38.5	10.8	45.9	13.5	0.618
	Random Forest	39.2	10.3	46.5	12.9	0.605
M. caribbica	Linear (Area + Env + Interactions, RidgeCV)	81.5	23.4	96.5	26.9	-0.573
	Elastic Net (poly2)	82.4	20.1	97.6	23.3	-0.604
	Gradient Boosting	70.2	18.6	81.5	22.0	-0.015
	Random Forest	66.1	17.2	75.9	20.6	-0.033
P. citrinum	Linear (Area + Env + Interactions, RidgeCV)	41.3	14.2	50.6	17.6	0.448
	Elastic Net (poly2)	40.6	13.5	49.9	17.0	0.463
	Gradient Boosting	29.1	9.8	34.6	11.5	0.762
	Random Forest	28.5	9.4	34.1	11.2	0.775

MAE – mean absolute error; RMSE – root mean squared error; R^2 – coefficient of determination; Env – environmental predictors (temperature and relative humidity).

Based on the results in Table 15, the best-performing model for each species is summarised in Table 16.

Table 16. Best model per species (summary)

Species	Best model	MAE (h)	RMSE (h)	R^2	No. of soups	No. of observations
C. cladosporioides	Gradient Boosting	38.5	45.9	0.618	6	108
M. caribbica	Random Forest	66.1	75.9	-0.033	3	67
P. citrinum	Random Forest	28.5	34.1	0.775	5	105

MAE – mean absolute error; RMSE – root mean squared error; R^2 – coefficient of determination.

To better understand the contribution of each predictor, Table 17 reports the relative feature importances in the best-performing model for each species.

Table 17. Feature importances in best models per species

Species	Feature	Importance
C. cladosporioides	Colony area	0.926
	Mean temp	0.066
	Mean RH	0.008
M. caribbica	Colony area	0.836
	Mean temp	0.084
	Mean RH	0.081
P. citrinum	Colony area	0.956
	Mean temp	0.022
	Mean RH	0.022

Feature importance is expressed as the proportion of variance explained by each predictor in the best-performing model. Mean temp – mean temperature; Mean RH – mean relative humidity

Using the best model per species, Table 18 presents the predicted elapsed time (in hours) for representative colony areas under average indoor environmental conditions.

Table 18. Predicted time (hours) at species-average environment

Species	Colony area (mm²)	Predicted time (h)
C. cladosporioides	1	125.1
	5	147.9
	10	136.3
	20	171.2
	30	191.1
M. caribbica	1	59.4
	5	83.1
	10	106.5
	20	148.9
	30	175.0
P. citrinum	1	60.2
	5	92.4
	10	118.6
	20	157.2
	30	186.7

Predicted time (hours) corresponds to species-average indoor environment values. Values are generated from the best model per species. Colony area expressed in mm².

Across all candidate species, machine learning models demonstrated variable capacity to predict elapsed time from colony area under indoor forensic conditions (Table 15). *P. citrinum* yielded the most accurate temporal estimates, with a random forest model achieving a MAE of 28.5 hours and R^2 of 0.775, indicating strong predictive validity. *C. cladosporioides* followed, with gradient boosting performing best (MAE 38.5 hours, R^2 0.618). In contrast, *M. caribbica* exhibited poor predictability (MAE 66.1 hours, R^2 near zero), limiting its forensic utility (Table 16).

Analysis of feature importances confirmed that colony area was the dominant predictor of time across all species, accounting for over 90% of variance in the best models (Table 17). T and RH contributed modestly, suggesting that while environmental factors play a role, the trajectory of colony expansion is the principal determinant of elapsed time.

The prediction grid (Table 18) illustrates the practical application of these models, providing expected temporal windows for given colony areas under species-average conditions. For example, a *P. citrinum* colony of 20 mm² corresponds to approximately 157 hours of growth,

with comparable colony areas in *C. cladosporioides* and *M. caribbica* predicting longer durations. These findings establish *P. citrinum* as the most reliable biomarker candidate for indoor temporal estimation, with *C. cladosporioides* serving as a viable secondary marker when present.

Figure 17 shows predictive surface plots of elapsed time as a function of colony area, T, and RH for *P. citrinum* under indoor conditions.

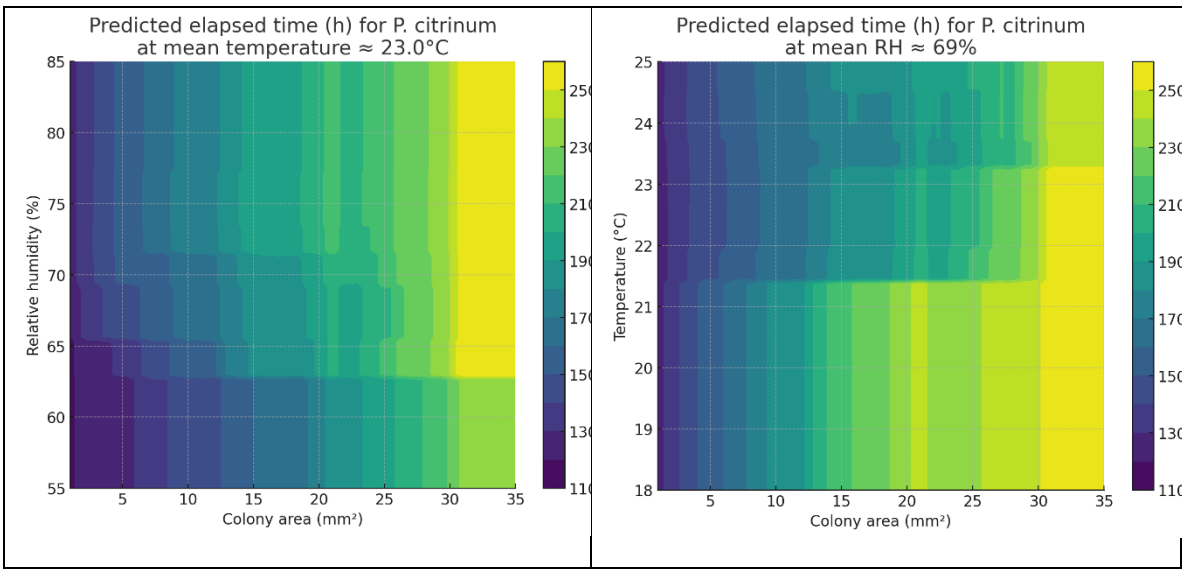

Figure 17. Predicted elapsed time (h) for *P. citrinum* as a function of colony area and temperature or relative humidity under indoor conditions at mean relative humidity (≈69%) or at mean temperature (≈23.0 °C). Contour lines depict modelled growth trajectories from the Random Forest estimator and illustrate the combined effect of colony expansion with temperature or moisture levels on temporal prediction.

The predictive surface plots (Figures 17) confirm that colony area is the dominant driver of temporal estimation for *P. citrinum*, with elapsed time increasing consistently as colonies expand. T exerted a modest accelerating effect at higher values, whereas RH produced comparatively weaker modulation of growth trajectories. To provide uncertainty estimates suitable for forensic application, quantile regression models were fitted to generate prediction intervals (Figure 18). The resulting 80% interval bands demonstrate that, although prediction uncertainty increases with colony size, the central estimates remain well constrained, reinforcing the practical reliability of *P. citrinum* as an indoor temporal biomarker.

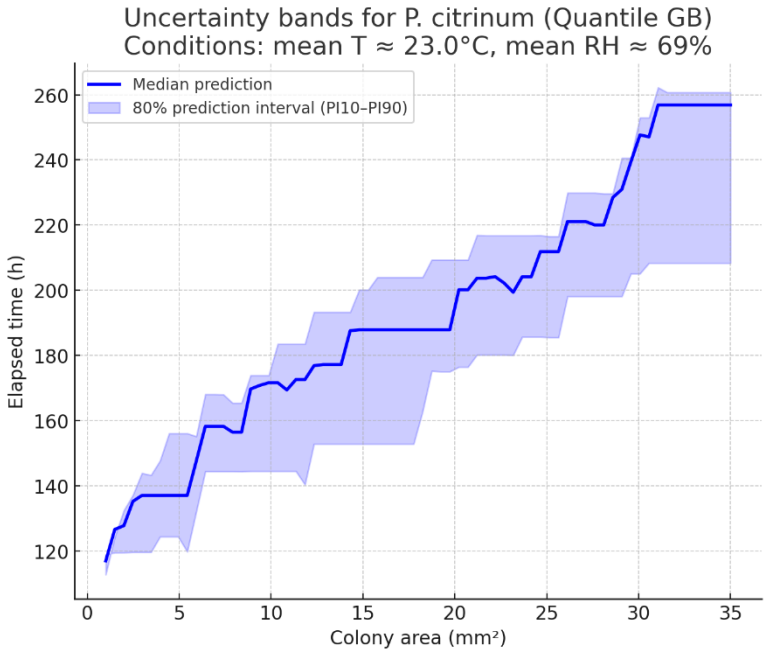

Figure 18. Uncertainty bands for *P. citrinum* predictions derived from quantile gradient boosting models. The blue line represents the median estimate, while the shaded region shows the empirical 80% prediction interval (PI10–PI90) under mean indoor conditions (temperature ≈23.0 °C; RH ≈69%).

4. Discussion

4.1 Species-Specific Growth Patterns on Soups and Bananas

This study demonstrates that different food substrates exhibit distinct fungal growth dynamics with forensic timing potential. In the soup assays, three fungi – *C. cladosporioides*, *M. caribbica*, and *P. citrinum* – were consistently observed, whereas the banana assays yielded *Fusarium verticillioides* (on ripe bananas) alongside *M. caribbica* and *P. citrinum* (Table 9; Figure 7). These organisms reflect varied ecological roles and time windows. *C. cladosporioides* attained the largest colonies in soups (up to ~106 mm²) and was present in all trials (Table 17; Figure 16), suggesting it is a robust early coloniser on nutrient-rich liquid substrates. In contrast, *M. caribbica* (a yeast) formed much smaller colonies (max. ~28 mm² in soup) and appeared in fewer replicates (Table 14), indicating an ephemeral presence – likely flourishing briefly on simple sugars before diminishing. *P. citrinum* showed intermediate behaviour in soup, with moderate colony sizes (~30 mm²) and detection in most samples (Table 14; Figure 16). On bananas, *F. verticillioides* was the dominant coloniser, capable of rapid and sustained growth (colonies >150 mm²) over long periods (up to ~156 days) (Table 9; Figure 7), whereas *M. caribbica* and *P. citrinum* on bananas remained spatially limited (colonies only a few mm²) and were confined to shorter post-exposure intervals (Table 9). These findings indicate distinct temporal colonisation patterns: fast-growing pioneer species (e.g. yeasts like *M. caribbica*) may briefly exploit readily available nutrients early on, followed by filamentous fungi that establish larger colonies and persist longer. The absence of *C. cladosporioides* on bananas and conversely of *F. verticillioides* on soup highlights how substrate type and initial microbial inocula drive species composition. Bananas, being acidic and plant-based, evidently favour fungi common in fruit decay (e.g. *Fusarium* spp.), whereas the complex ingredients and neutral pH of soup provided a niche for environmental molds like *Cladosporium*. Such differences are consistent with known spoilage ecology: fruits with low pH tend to select for acid-tolerant fungi (e.g. *Penicillium*, *Cladosporium*), while protein-rich, less acidic matrices can support a broader range of microbes including bacteria (Zhao et al., 2020). Importantly, each fungal species' presence (or absence) and colony size can be mapped to an approximate time range since abandonment. For instance, detection of only small *M. caribbica* colonies might indicate an early stage (a few days), whereas a vigorous *F. verticillioides* infestation on a banana implies

a much longer interval (several weeks or more). These species-specific time frames reflect predictable fungal growth dynamics on different food substrates, similar to a microbial "clock" as has been documented in cadaver studies where predictable microbial community shifts occur over time (Finley et al., 2015; Metcalf et al., 2013). Our results extend this paradigm to common food items, corroborating that the fungal community composition on a substrate can serve as a chronological indicator in indoor environments.

4.2 Performance of Chronological Modelling Approaches

For time prediction from OD, the linear model (OLS with OD^2 and interaction terms) provided the best CV performance (MAE = 91.1 h; $R^2 = 0.756$) (Table 7), whereas for colony-area prediction, ensemble models performed better (Tables 15–16). Hence, model selection should depend on the prediction target and substrate type. Therefore, model superiority should be qualified by substrate and target variable. In the soup dataset, simple inverse-linear models (even with polynomial terms and interactions) had limited predictive power – for example, linear ridge regression yielded low or even negative R^2 for *C. cladosporioides* and *M. caribbica*, indicating it often underfit the sigmoidal growth patterns. The penalised elastic net performed similarly poorly (e.g. R^2=-0.60 for *M. caribbica*), suggesting that mild regularisation did not remedy the mismatch between linear assumptions and biological reality. By contrast, ensemble tree-based models captured the non-linear growth–time relationships more effectively. Gradient boosting and random forests achieved the best performance for most species in soup, with *C. cladosporioides* and *P. citrinum* models reaching R^2 approx 0.60 and substantially lower error margins than linear models. This improvement reflects the ability of tree ensembles to accommodate interaction effects and threshold behaviours (e.g. rapid initial expansion followed by plateau) that characterise microbial colony growth. That said, even the best soup models had prediction errors on the order of tens of hours, which is non-trivial for forensic purposes.

On bananas, all modelling approaches struggled, although the subset of assays conducted under controlled temperature conditions helped reduce temperature-related uncertainty, highlighting the greater challenge of predicting time over longer and more heterogeneous intervals. The extreme temporal span of the banana trials (15–57 days) and the saturation of the banana peel's optical signal limited model accuracy. For *F. verticillioides* (which grew

over months in one case), even a flexible gradient boosting model yielded a very poor fit (MAE ≈ 531 hours, R^2 strongly negative), essentially failing to account for the massive variation in colony development times. *M. caribbica* and *P. citrinum* on banana also proved difficult to model: their narrower growth windows produced slightly better R^2 (up to ~0.24 for *P. citrinum* with random forest) but still large errors on the order of 160–200 hours. Overall, predictive accuracy on bananas was substantially poorer than on soups. The mechanistic two-stage modelling (logistic/Hill growth curve fitting with subsequent regression of curve parameters on environment) provided useful biological insight – confirming, for example, that warmer/drier conditions accelerated the optical ripening curves – but did not dramatically improve predictive precision for unseen cases. A threshold-based AFT approach similarly yielded broad time estimates with wide confidence bounds. In essence, the inherent variability in banana decomposition under different microclimates imposed a hard limit on prediction accuracy. Our modelling results therefore emphasise that straightforward regression may be inadequate for long-term or highly non-linear growth data. Ensemble methods and non-parametric models are better suited to capture complex trajectories, but even these require extensive training data to encompass all sources of variability. In future applications, incorporating larger datasets and additional predictors (e.g. chemical byproducts of decay) might improve precision. Although some models showed reasonable performance in soup experiments simulating short post-abandonment intervals, the practical forensic adoption should be restricted to providing complementary estimates with broad confidence intervals and caution against deterministic interpretations. For longer intervals evidenced by mummified foods, alternate approaches – perhaps identifying stage-specific microbial biomarkers rather than relying on continuous growth metrics – may be more reliable.

4.3 Influence of Environmental Conditions

Our findings reinforce that indoor environmental conditions, especially T and RH, critically influence microbial growth rates and temporal development patterns. Even within the relatively stable indoor ranges of this study, subtle differences altered the timeline of decomposition. T emerged as the dominant factor governing fungal activity. Bananas stored in cooler conditions (e.g. averaging ~14 °C) decomposed slower and supported protracted fungal growth, whereas those in warm settings (~26–30 °C) ripened and decayed quickly –

in some cases so rapidly that visible mold colonies did not have time to develop before the substrate was exhausted. Importantly, a subset of banana assays was conducted under controlled temperature conditions (26 °C), which reduced thermal variability and allowed a clearer assessment of temperature effects on fungal growth dynamics. Indeed, we observed *P. citrinum* and *M. caribbica* colonising bananas only at moderate T (15–21 °C), whereas at 26–30 °C no fungal colonies were observed on the bananas. This temperature-dependent inhibition is consistent with fundamental microbiology: each species has an optimal T range for enzyme function and growth, and significant deviation (either too low or too high) can halt proliferation (Nedwell, 2006). High T can denature fungal enzymes and may also inhibit bacterial proliferation, effectively limiting overall microbial colonisation despite ample nutrients (Jay et al., 2005). Conversely, low T (e.g. ~3–5 °C in one extreme case) drastically slow metabolic activity, extending the time needed for any observable decay (Nedwell, 2006). These principles align with prior forensic research showing that cooler environments delay decomposition, while moderate warmth accelerates it (Carter et al., 2007).

RH is another key factor, as it influences water availability in the substrate. Fungi generally require a minimum water activity to germinate and grow, and ambient humidity affects how quickly a food item desiccates. In our indoor trials, humidity ranged from ~45% to >90% depending on location. We found that sufficient ambient humidity helped sustain microbial activity: for instance, extremely arid conditions were not part of our study, but literature suggests that if humidity drops too low, fungal growth will pause even if T is favourable (Pitt et al., 2009). In the present work, environments with higher RH tended to prolong the active growth phase (as the food did not dry out as fast), whereas moderately low humidity (≈45–50%) in warm rooms led to quicker drying of both soup and banana surfaces, potentially shortening the window of mold expansion. Notably, our model feature importance analysis indicated that for *F. verticillioides* on bananas, T and RH together accounted for over half of the variance in time predictions, outweighing the colony size effect. This suggests that *Fusarium*'s growth was highly sensitive to the environment – e.g. thriving for months under cool, humid conditions, but completing its life cycle much faster (or failing to sporulate) under warmer or drier conditions. By contrast, *M. caribbica* and *P. citrinum* showed colony size as the primary time determinant with a more modest environmental influence, implying those species have narrower physiological tolerances and will only grow at all under a fairly

specific range of indoor conditions. In forensic terms, this means the same species can indicate very different times since abandonment depending on the ambient conditions. Investigators must therefore consider the scene environment – for example, a heated dry apartment vs. a cool damp cellar – when interpreting microbial evidence. Wherever possible, measuring or estimating the T/RH history of the scene (for instance, via HVAC records or dataloggers) will improve the accuracy of time since abandonment estimates derived from microbial growth (Carter et al., 2010). Ultimately, our study underlines that indoor decomposition follows more predictable trajectories than outdoor scenarios, because indoor climates are less variable (Carter et al., 2007), but even modest indoor climate differences can shift the microbial timeline significantly. Models aiming to serve as "microbial chronometers" must incorporate these factors, perhaps by treating T/RH as covariates as we did, or by normalising growth rates to a standard reference condition (Rousk et al., 2009).

4.4 Substrate Effects on Microbial Development and Growth Dynamics

The contrasting results between soup and banana substrates highlight how the physical and chemical nature of a substrate shapes decomposition. Banana is a solid, fibrous matrix with an intact peel that initially slows microbial ingress; it has high sugar content, low pH (around 4.5–5), and undergoes a climacteric ripening process. In our experiments the banana peel itself darkened from yellow to black as starches converted to sugars and microbial colonisation took hold – an optical ripening marker we quantified as the mean grey value OD of the peel. Soups, on the other hand, are liquid or semi-liquid emulsions of diverse ingredients, near-neutral in pH, with very high water activity but prone to surface drying. These fundamental differences resulted in distinct microbial ecosystems. The banana peel acted as a barrier early on, so initial microbial growth (often yeast) occurred in localized breaches or on the cut stem end, until the peel became overripe. As the banana ripened and the peel's defences broke down, molds like *Fusarium* and *Penicillium* proliferated, feeding on the abundant simple sugars and moist pulp beneath the peel. The optical measurements captured this transition: peel OD rose steadily as the banana browned and colonising mycelia spread underneath. Eventually, in humid conditions, the peel itself became overgrown with mycelium, whereas in drier air it simply mummified. The soup allowed more immediate and widespread colonisation, since its surface was exposed and already at optimal moisture. Fungal spores settling from air could germinate on the nutrient-rich broth within hours. We

observed that even when stored uncovered, soups typically supported only a few dominant colonies (often *Cladosporium* or *Penicillium*), rather than a uniform mold carpet – likely because once a colony establishes, it locally depletes nutrients and may produce inhibitory metabolites that prevent other fungi from taking over the same soup (a form of microbial competition). The soup's liquid nature also means microbes can diffuse, potentially accelerating initial decay but also causing the substrate to exhaust or stabilize faster than a solid fruit. In our data, mold growth in soups tended to plateau within 10–12 days (with colony areas reaching a maximum and then little expansion), presumably as nutrients were consumed or the broth dried/thickened, effectively limiting the detectable temporal progression of microbial growth to a short timeframe. Bananas, in contrast, showed signs of microbial activity for much longer under favourable conditions – even after the peel fully blackened, *F. verticillioides* continued to slowly enlarge its colonies, suggesting that the fruit's cellulose-rich tissues supported prolonged fungal metabolism. From a forensic perspective, using multiple substrates can extend the overall window of estimation. A fresh or lightly spoiled soup bowl might indicate abandonment on the order of days, whereas a completely rotted banana in the same scene might point to weeks; taken together, they provide a more complete timeline of events. Moreover, substrate differences in microbial succession offer CV: if all available foods, regardless of type, show advanced colonisation, one can infer a longer absence (or higher ambient T) than if only one substrate is heavily decomposed while others remain relatively intact. This reinforces the value of examining any and all perishable food remnants at a scene – each item's state of decay is a piece of the temporal puzzle. Our results justify the selection of both a liquid (soup) and a solid (banana) in this study, as their complementary characteristics illustrate the range of microbial chronometers that domestic foods can provide.

4.5 Ecological Interpretation of Fungal Growth Patterns

Considering the broader ecological context helps interpret why these predictable fungal growth patterns occur and how reliable they may be as temporal indicators. The fungi observed are all ubiquitous saprotrophs well-adapted to colonise rich organic matter. *C. cladosporioides* and *P. citrinum* are early-stage colonisers often found on plant material and foods; they produce abundant airborne conidia that readily germinate on exposed surfaces (Hawksworth et al., 2011). Their rapid appearance on our samples aligns with their ecological

strategy to exploit new nutrient sources quickly. *M. caribbica*, identified in both substrates, is a yeast associated with fermenting plant materials – its transient presence likely corresponds to the fermentation of sugars in the initial days. Being unicellular and fast-replicating, yeasts can surge in population and then decline once simple sugars are depleted or when conditions (pH, alcohol content, etc.) become unfavourable. In contrast, *F. verticillioides* represents a late-stage coloniser on the banana: this species (a known plant pathogen and spoilage mold) can degrade more complex polymers like cellulose and pectin, enabling it to persist on the banana long after simpler nutrients are gone. The protracted growth of *Fusarium* in cool, humid conditions suggests a slow but steady enzymatic breakdown of the fruit, reflecting a strategy for long-term resource utilisation. These observations are consistent with well-established ecological differences in fungal growth strategies and substrate utilisation during decomposition, where communities transition from r-strategists (fast-growing opportunists) to K-strategists (slower-growing but resilient organisms) over time (Pitt et al., 2009). From a forensic standpoint, this means early versus late indicators have different reliability: early-stage microbes (like *M. caribbica* or *C. cladosporioides* in our study) can confirm that only a short time has passed since exposure – but if conditions were suboptimal they might never appear at all. Late-stage fungi (like *F. verticillioides* or robust *P. citrinum* colonies) confirm a substantial interval has elapsed, yet once they dominate, it becomes harder to pinpoint how much beyond a minimum threshold (e.g. a fully overgrown banana could be 3 weeks or 3 months old, depending on climate). This ceiling effect was evident in our banana models, where elapsed time predictions saturated beyond a certain colony size or OD, yielding wide uncertainty for the longest intervals. It underlines an ecological reality: decomposition does not progress indefinitely in a linear fashion – it eventually enters a steady state where most readily available nutrients are consumed and microbial activity plateaus (Manzoni et al., 2023). For forensic science, this suggests diminishing returns when estimating very long post-abandonment periods using microbial growth alone. Future studies incorporating broader molecular approaches may help refine species-level resolution and improve the temporal interpretability of fungal growth patterns across diverse substrates. Finally, the integration of morphological identification with molecular confirmation (Schoch et al., 2012; White et al., 1990). Strengthens ecological reliability: morphologically similar fungi can occupy the same niche (for instance, several

Penicillium or *Aspergillus* species appearing as green moulds on food), meaning that without DNA identification there is a risk of species misidentification and, consequently, misinterpretation of the temporal growth phase. Classical mycology texts (Ellis, 2007; Walsh et al., 2018). Note the difficulty of distinguishing species by appearance alone, particularly in mixed colonies. By sequencing the isolates, we ensured that the observed successional signals were genuine rather than artefacts of misidentification. This approach reinforces the ecological and forensic validity of using fungal growth patterns in food remains, as it ensures that the observed temporal signals reflect genuine species-specific growth dynamics shaped by the substrate ecology rather than artefacts of morphological ambiguity (Hawksworth et al., 2015).

4.6 Forensic Applicability and Limitations

Our results have direct implications for forensic investigations of indoor scenes, especially those involving delayed discovery of human remains or evidence of prolonged neglect. The temporal development of fungal growth on common foods offers a novel proxy to estimate the time since human activity ceased in a dwelling. Traditional post-mortem interval estimations often falter indoors due to the lack of insect evidence or altered cadaveric changes (Amendt et al., 2011; Henssge et al., 2004). In such cases, something as unassuming as a moldy bowl of soup or an overripe banana on a countertop can provide vital temporal clues. Despite the promising results, several limitations must be acknowledged. First, environmental conditions in domestic settings are inherently heterogeneous, and even small differences in T, RH, ventilation, or light exposure can substantially affect fungal growth rates and temporal development patterns. Consequently, extrapolating timelines across different residences or rooms may introduce significant uncertainty. Second, the predictive accuracy of fungal growth–based timing approaches is constrained by substrate-specific dynamics; for instance, banana trials demonstrated saturation of optical signals and prolonged decomposition, leading to wide prediction intervals for long-term estimations. Third, human interference—such as moving, microwaving, or partially consuming the food—can reset or alter microbial development, potentially confounding time estimates. Regional and situational variability in fungal communities must also be considered, as species composition may differ between households or climates, limiting the generalisability of the results. Finally, this approach should be viewed as a complementary tool, rather than

a standalone method, to support traditional post-mortem interval estimation or investigation of neglect; temporal ranges should be interpreted as broad intervals rather than precise time points. Incorporating these considerations, future studies should aim to develop standardised protocols, larger datasets, and reference microbial chronograms to improve reliability and applicability in forensic casework. For example, the mere presence of a particular fungus can narrow the window: finding associated with short post-exposure intervals (like a thin layer of *C. cladosporioides* on leftovers) might suggest the food was exposed for just a few days, whereas a predominant *F. verticillioides* infestation points to a much longer period. Investigators can compare the scene's microbial evidence with our experimental data to infer time frames. If, say, a banana at a crime scene is completely black and supports abundant *F. verticillioides*, one might reasonably infer that the residence was abandoned for several weeks at least – especially if ambient conditions were cool. Likewise, a dry soup pot with only dormant mold spores might indicate it had sat undisturbed for over two weeks (long enough for the soup to dehydrate and active growth to cease). These kinds of interpretations, while qualitative, add a new line of evidence to time-of-abandonment estimations, complementing other clues such as spoiled groceries, accumulated mail, or appliance timers. However, it is important to acknowledge the limitations and necessary precautions when applying this method. Predictive accuracy proved limited (mean errors on the order of days), which requires caution in a forensic context. Its use is recommended only as a complementary tool, integrated with other methods (entomology, physical chemistry). In a real case, where the prior temperature and humidity might not be recorded and microbial inoculation is chance-driven, the uncertainty would be higher. Thus, any time estimate derived from microbial succession should be given as a broad range, not an exact point estimate. For instance, we can say "at least 1–2 weeks" rather than "exactly 10 days" based on a given mold growth stage. Second, regional and situational variability in microbial presence must be considered. The fungi in our study are cosmopolitan, but microbial biogeography means other species might dominate in different homes or climates (Weçoski et al., 2023). Investigators should ideally sample the specific colonies and identify them (through morphological keys or DNA sequencing) rather than assume they are the same species we observed. In practice, this calls for forensic mycology protocols: sterile swabbing of food molds, culturing or direct DNA analysis, and comparison with a reference database of

succession timelines for identified species. Building such databases – analogous to entomological PMI databases – is a crucial next step. Third, the method assumes the food was not disturbed or moved during the post-abandonment interval. If a perpetrator microwaved the soup after the victim's disappearance or if a window was left open altering the environment, the fungal growth timeline could be reset or altered. Careful scene investigation is needed to rule out such confounders. Despite these limitations, the approach is fundamentally sound as supported by our empirical data and aligns with the growing body of evidence that microbes can function as temporal evidence in forensic contexts (Hawksworth et al., 2015; Metcalf et al., 2013). Notably, our study used methods accessible to many forensic laboratories – visual observation, image analysis, culture, and basic molecular sequencing – avoiding the need for expensive high-throughput metagenomics (Nam et al., 2023). This increases the practicality of adopting analysis of fungal growth patterns in routine casework. It provides a template for developing standard operating procedures for forensic examination of perishable foods and other microbial substrates at crime scenes. With appropriate validation, a forensic scientist could one day testify that "the mold growth on the kitchen food indicates the house was likely unoccupied for approximately X days," adding an objective backing to timeline reconstruction.

5. Conclusion

In summary, this work demonstrates that the chronological progression of microbial and optical changes in common foods can be harnessed to estimate time-since-abandonment in indoor settings. Bananas and vegetable soup – representative of solid and liquid food residues – each exhibited a predictable temporal progression of fungal growth and measurable optical decay markers that correspond to post-exposure intervals. We found that *C. cladosporioides*, *P. citrinum*, and yeast colonisation in soup can indicate spoilage on the order of days to a couple of weeks, while on bananas a transition from early yeast activity to extensive *F. verticillioides* growth signals a longer period (weeks to months, depending on climate).

Multiple modelling approaches (ridge regression, elastic net, random forests, gradient boosting, and mechanistic growth models) were applied to quantify these relationships, highlighting both the promise and the current limitations of microbial timekeepers. Environmental factors proved critical: indoor temperature and humidity modulate the pace of decomposition, such that time estimates must be contextualised for the scene's conditions. Substrate properties (pH, water content, structure) select for different microbial communities and decay trajectories, reinforcing that a multi-substrate approach broadens the effective post-abandonment timeframe that can be assessed.

The forensic value of these findings lies in providing investigators with an additional, science-based tool to infer how long a space has been left undisturbed, particularly when traditional indicators are unavailable. By integrating microbiological evidence – visible colony growth, species identification, and quantitative models – forensic timelines can be made more robust, especially in clandestine scenarios such as sealed apartments or cases of neglect.

This study provides a proof-of-concept that microbial and optical changes in common substrates may help estimate time-since-abandonment under indoor conditions. However, predictive accuracy varies widely across species and substrates (MAE ≈ 28–531 h). Therefore, conservative, species- and substrate-specific estimates should be preferred until further field validation is achieved.

Future research should integrate multiomics analyses (metagenomics, metabolomics), expand to different foods, and validate models in simulated crime scene scenarios. As

successional patterns may vary with geography or microclimate, extensive reference data and casework validation will be essential before microbial clocks become reliable forensic tools.

Recommendations for forensic implementation**:** standardized protocols are essential, including sterile swabbing of mold colonies, photographic documentation of food items, controlled transport and preservation, and timely microbiological analysis at the lab. Development of reference microbial chronograms and integration with environmental records (temperature, humidity) will enhance reliability. Simulating real crime scene conditions, including mixed substrates and background contamination, will further validate predictive models. Establishing these procedures will be critical for forensic admissibility and practical application in casework.

In conclusion, fungal growth patterns on indoor food remains is a promising chronotaphonomic indicator that broadens the forensic toolkit for timing events. Our study provides a foundational understanding of fungal and visual decay progression on two common substrates, offering both proof of concept and a springboard for advancing forensic chronometry using the smallest of organisms.

6. References

Alegbeleye, O., Odeyemi, O. A., Strateva, M., & Stratev, D. (2022). Microbial spoilage of vegetables, fruits and cereals. In Applied Food Research (Vol. 2, Issue 1). Elsevier B.V. doi: 10.1016/j.afres.2022.100122

Amendt, J., Richards, C. S., Campobasso, C. P., Zehner, R., & Hall, M. J. R. (2011). Forensic entomology: Applications and limitations. *Forensic Science, Medicine, and Pathology*, *7*(4), 379–392. doi: 10.1007/s12024-010-9209-2

Andrade, I. L. de. (2024). Micologia forense aplicada em investigações criminais: Uma revisão. *Revista Foco*, *17*(7), e5769. doi: 10.54751/revistafoco.v17n7-147

Ben-Dov, E., Shapiro, O. H., Siboni, N., & Kushmaro, A. (2006). Advantage of using inosine at the 3′ termini of 16S rRNA gene universal primers for the study of microbial diversity. *Applied and Environmental Microbiology*, *72*(11), 6902–6906. doi: 10.1128/AEM.00849-06

Campos, C. (2018). *Avaliação da termorresistência de Bacillus cereus em preparados de cereais com base na variação da temperatura, pH e atividade da água* [Tese de Mestrado]. Universidade do Minho.

Carter, D. O., Yellowlees, D., & Tibbett, M. (2007). Cadaver decomposition in terrestrial ecosystems. In Naturwissenschaften (Vol. 94, Issue 1, pp. 12–24). doi: 10.1007/s00114-006-0159-1

Carter, D. O., Yellowlees, D., & Tibbett, M. (2010). Moisture can be the dominant environmental parameter governing cadaver decomposition in soil. *Forensic Science International*, *200*(1–3), 60–66. doi: 10.1016/j.forsciint.2010.03.031

Eisenhofer, R., Minich, J. J., Marotz, C., Cooper, A., Knight, R., & Weyrich, L. S. (2019). Contamination in Low Microbial Biomass Microbiome Studies: Issues and Recommendations. In Trends in Microbiology (Vol. 27, Issue 2, pp. 105–117). Elsevier Ltd. doi: 10.1016/j.tim.2018.11.003

Ellis, David. (2007). *Descriptions of medical fungi* (2nd ed.). Nexus Print Solutions.

Finley, S. J., Benbow, M. E., & Javan, G. T. (2015). Microbial communities associated with human decomposition and their potential use as postmortem clocks. In International Journal of Legal Medicine (Vol. 129, Issue 3, pp. 623–632). doi: 10.1007/s00414-014-1059-0

Gandra, E. Á., Gandra, T., Mello, W., & Godoi, H. (2008). Técnicas moleculares aplicadas à microbiologia de alimentos. *Acta Scientiarum. Technology*, *30*(1), 109–118. doi: 10.4025/actascitechnol.v30i1.3245

García-Descalzo, L., García-López, E., & Cid, C. (2022). Comparative Proteomic Analysis of Psychrophilic vs. Mesophilic Bacterial Species Reveals Different Strategies to Achieve Temperature Adaptation. *Frontiers in Microbiology*, *13*. doi: 10.3389/fmicb.2022.841359

Guo, X., Gu, L., Luo, Y., Wang, S., Luo, H., & Song, F. (2023). A bibliometric analysis of microbial forensics from 1984 to 2022: progress and research trends. In Frontiers in Microbiology (Vol. 14). Frontiers Media S.A. doi: 10.3389/fmicb.2023.1186372

Hawksworth, D. L., & Wiltshire, P. (2015). Forensic mycology: current perspectives. *Research and Reports in Forensic Medical Science*, *5*, 75–83. doi: 10.2147/rrfms.s83169

Hawksworth, D. L., & Wiltshire, P. E. J. (2011). Forensic mycology: The use of fungi in criminal investigations. In Forensic Science International (Vol. 206, Issues 1–3, pp. 1–11). doi: 10.1016/j.forsciint.2010.06.012

Helgi Library. (2021). *Banana Consumption Per Capita – Portugal*. Retrieved from https://www.helgilibrary.com/indicators/banana-consumption-per-capita/portugal/

Henssge, C., & Madea, B. (2004). Estimation of the time since death in the early post-mortem period. *Forensic Science International*, *144*(2–3), 167–175. doi: 10.1016/j.forsciint.2004.04.051

Jay, J., Loessner, M., & Golden, D. (2005). *Modern Food Microbiology* (7th ed.). Springer.

Manzoni, S., Chakrawal, A., & Ledder, G. (2023). Decomposition rate as an emergent property of optimal microbial foraging. *Frontiers in Ecology and Evolution*, *11*. doi: 10.3389/fevo.2023.1094269

Martins, C. (2022). *Controle de fungos associados á linha de processamento de suco de laranja* [Tese de Mestrado]. Universidade Estatual de Campinas.

Mathur, A., & Agrawal, Y. K. (2011). An overview of methods used for estimation of time since death. *Australian Journal of Forensic Sciences*, *43*(4), 275–285. doi: 10.1080/00450618.2011.568970

Metcalf, J. L., Wegener Parfrey, L., Gonzalez, A., Lauber, C. L., Knights, D., Ackermann, G., Humphrey, G. C., Gebert, M. J., Van Treuren, W., Berg-Lyons, D., Keepers, K., Guo, Y., Bullard, J., Fierer, N., Carter, D. O., & Knight, R. (2013). A microbial clock provides an accurate estimate of the postmortem interval in a mouse model system. *ELife*, *2*. doi: 10.7554/elife.01104

Nam, N. N., Do, H. D. K., Loan Trinh, K. T., & Lee, N. Y. (2023). Metagenomics: an effective approach for exploring microbial diversity and functions. In Foods (Vol. 12, Issue 11). doi: 10.3390/foods12112140

Nedwell, D. B. (2006). Effect of low temperature on microbial growth: lowered affinity for substrates limits growth at low temperature. *FEMS Microbiology Ecology*, *30*(2), 101–111. doi: 10.1111/j.1574-6941.1999.tb00639.x

Nodari, R., Arghittu, M., Bailo, P., Cattaneo, C., Creti, R., Aleo, francesco, Saegeman, V., Franceschetti, L., Novati, S., Fernandez-Rodrigues, A., Verzeletti, A., Farina, C., & Bandi, C. (2024). Forensic Microbiology: When, Where and How. In Microorganisms (Vol. 12, Issue 5). Multidisciplinary Digital Publishing Institute (MDPI). doi: 10.3390/microorganisms12050988

Oliveira, M. V. S. de, Silva, R. C., & Rodrigues, F. M. (2023). Verificação dos padrões globais do conhecimento científico sobre a microbiologia forense. In Luis Guillermo Ramírez Mérida (Ed.), Microbiologia: perspectivas em saúde e alimentação (pp. 106–126). Canoas: Mérida Publishers. doi: 10.4322/mp.978-65-84548-16-9.c5

Pechal, J. L., Crippen, T. L., Benbow, M. E., Tarone, A. M., Dowd, S., & Tomberlin, J. K. (2014). The potential use of bacterial community succession in forensics as described by high throughput metagenomic sequencing. *International Journal of Legal Medicine*, *128*(1), 193–205. doi: 10.1007/s00414-013-0872-1

Pitt, J. I., & Hocking, A. D. (2009). Fungi and food spoilage. In Fungi and Food Spoilage (3rd ed.). Springer US. doi: 10.1007/978-0-387-92207-2

Robinson, J. M., Pasternak, Z., Mason, C. E., & Elhaik, E. (2021). Forensic Applications of Microbiomics: A Review. In Frontiers in Microbiology (Vol. 11). Frontiers Media S.A. doi: 10.3389/fmicb.2020.608101

Rousk, J., Brookes, P. C., & Bååth, E. (2009). Contrasting soil pH effects on fungal and bacterial growth suggest functional redundancy in carbon mineralization. *Applied and Environmental Microbiology*, *75*(6), 1589–1596. doi: 10.1128/AEM.02775-08

Schneider, C. A., Rasband, W. S., & Eliceiri, K. W. (2012). NIH Image to ImageJ: 25 years of image analysis. In Nature Methods (Vol. 9, Issue 7, pp. 671–675). doi: 10.1038/nmeth.2089

Schoch, C. L., Seifert, K. A., Huhndorf, S., Robert, V., Spouge, J. L., Levesque, C. A., Chen, W., Bolchacova, E., Voigt, K., Crous, P. W., Miller, A. N., Wingfield, M. J., Aime, M. C., An, K. D., Bai, F. Y., Barreto, R. W., Begerow, D., Bergeron, M. J., Blackwell, M., … Schindel, D. (2012). Nuclear ribosomal internal transcribed spacer (ITS) region as a universal DNA barcode marker for Fungi. *Proceedings of the National Academy of Sciences of the United States of America*, *109*(16), 6241–6246. doi: 10.1073/pnas.1117018109

Walsh, T. H., Hayden, R. T., & Larone, D. H. (2018). *Larone´s medically Important Fungi a guide to identification* (6th ed.). ASM Press. Retrieved from https://lccn.loc.gov/2018015129

Weçoski, D. A. D., & Dalzoto, P. (2023). Microbiologia Forense: uma revisão. *Revista Brasileira de Criminalística*, *12*(2), 112–121. doi: 10.15260/rbc.v12i2.572

White, T. J., Bruns, S. B., Lee, & Taylor, J. W. (1990). Amplification and direct sequencing of fungal ribosomal RNA Genes for phylogenetics. In In M. A. Innis, D. H. Gelfand, J. J. Sninsky, & T. J. White (Eds.), PCR protocols: A guide to methods and applications (pp. 315–322). Academic Press. Retrieved from https://www.researchgate.net/publication/223397588

Zhao, P., Ndayambaje, J. P., Liu, X., & Xia, X. (2020). Microbial Spoilage of Fruits: A Review on Causes and Prevention Methods. *Food Reviews International*, *38*(S1), 225–246. doi: 10.1080/87559129.2020.1858859

Annex

Molecular Identification of Fungal Isolates

The molecular identification of fungal isolates obtained from banana and soup samples was performed by sequencing the ITS (Internal Transcribed Spacer) region, followed by BLAST analysis against the NCBI GenBank database. The sequences obtained and their corresponding chromatograms are presented below, along with the alignment results of the closest database matches.

The following sequence corresponds to the ITS region of the isolate identified as *Penicillium citrinum*, obtained from banana and soup samples.

GGGTAANAGAGNTGCGGGCCCTCGGGGCCAACCTCCCACCCGTGTTGCCCG
AACCTATGTTGCCTCGGCGGGCCCCGCGCCCGCCGACGGCCCCCCTGAACG
CTGTCTGAAGTTGCAGTCTGAGACCTATAACGAAATTAGTTAAAACTTTCAACA
ACGGATCTCTTGGTTCCGGCATCGATGAAGAACGCAGCGAAATGCGATAACT
AATGTGAATTGCAGAATTCAGTGAATCATCGAGTCTTTGAACGCACATTGCGC
CCTCTGGTATTCCGGAGGGCATGCCTGTCCGAGCGTCATTGCTGCCCTCAAG
CCCGGCTTGTGTGTTGGGCCCCGTCCCCCCCGCCGGGGGGACGGGCCCGA
AAGGCAGCGGCGGCACCGCGTCCGGTCCTCGAGCGTATGGGGCTTCGTCAC
CCGCTCTAGTAGGCCCGGCCGGCGCCAGCCGACCCCCAACCTTTAATTATCT
CAGGTTGACCTCGGATCAGGTAGGGATACCCGCTGAACTTAAGCATATCAATA
AGCCGGAGGAA

The chromatogram (Figure 1A) illustrates the high-quality base calls obtained during sequencing.

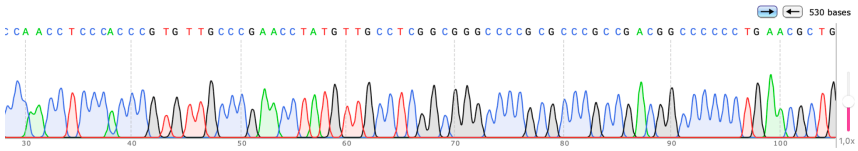

Figure 1A. Chromatogram of the ITS region sequence from *P. citrinum*.

The following sequence corresponds to the ITS region of the isolate identified as *Meyerozyma caribbica*, obtained from both banana and soup samples.

GGGTAATAGAATTCTTTTGCCAGCGCTTAACTGCGCGGCGAAAACCTTACACA
CAGTGTCTTTTTGATACAGAACTCTTGCTTTGGTTTGGCCTAGAGATAGGTTG
GGCCAGAGGTTTAACAAAACACAATTTAATTATTTTTATTGATAGTCAAATTTTG
AATTAATCTTCAAAACTTTCAACAACGGATCTCTTGGTTCTCGCATCGATGAAG
AACGCAGCGAAATGCGATAAGTAATATGAATTGCAGATTTTCGTGAATCATCG
AATCTTTGAACGCACATTGCGCCCTCTGGTATTCCAGAGGGCATGCCTGTTTG
AGCGTCATTTCTCTCTCAAACCCCCGGGTTTGGTATTGAGTGATACTCTTAGT
CGAACTAGGCGTTTGCTTGAAAAGTATTGGCATGGGTAGTACTGGATAGTGCT
GTCGACCTCTCAATGTATTAGGTTTATCCAACTCGTTGAATGGTGTGGCGGGA
TATTTCTGGTATTGTTGGCCCGGCCTTACAACAACCAAACAAGTTTGACCTCA
AATCAGGTAGGAATACCCGCTGAACTTAAGCATATCAATAAGCCGGAGGAA

The chromatogram (Figure 2A) confirms the sequencing quality

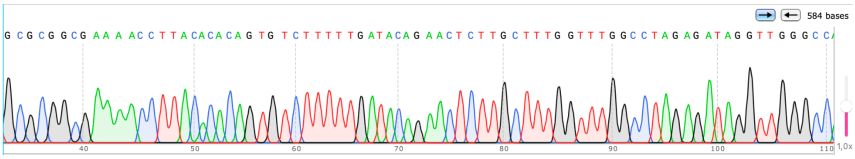

Figure 2A. Chromatogram of the ITS region sequence from *M. caribbica.*

The ITS sequence obtained from the banana sample corresponded to *Fusarium verticillioides*.

GGGACGGGATCTANCCTGATCCGAGGTCAACATTCAGAAGTTGGGGTTTAAC
GGCGTGGCCGCGACGATTACCAGTAACGAGGGTTTTACTACTACGCTATGGA
AGCTCGACGTGACCGCCAATCAATTTGGGGAACGCGATTTGACTCGCGAGTC

CCAACACCAAGCTGGGCTTGAGGGTTGAAATGACGCTCGAACAGGCATGCCC
GCCAGAATACTGGCGGGCGCAATGTGCGTTCAAAGATTCGATGATTCACTGA
ATTCTGCAATTCACATTACTTATCGCATTTTGCTGCGTTCTTCATCGATGCAAA
A

The chromatogram (Figure 3A) displays the nucleotide sequence with minimal ambiguity, confirming the accuracy of the result.

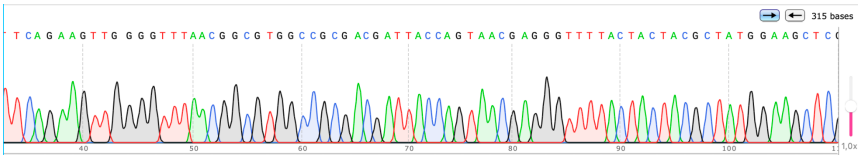

Figure 3A. Chromatogram of the ITS region sequence from *F. verticillioides.*

The following ITS region sequence was obtained from the soup sample and identified as *Cladosporium cladosporioides*.

GGGNGGTTCCTACCTGATCCGAGGTCAACCTTAGAAATGGGGTTGTTTTACG
GCGTAGCCTCCCGAACACCCTTTAGCGAATAGTTTCCACAACGCTTAGGGGA
CAGAAGACCCAGCCGGTCGATTTGAGGCACGCGGCGGACCGCGTTGCCCAA
TACCAAGCGAGGCTTGAGTGGTGAAATGACGCTCGAACAGGCATGCCCCCC
GGAATACCAGGGGGCGCAATGTGCGTTCAAAGATTCGATGATTCACTGAATT
CTGCAATTCACATTACTTATCGCATTTCGCTGCGTTCTTCATCGATGCCAGAAC
CAAGAGATCCGTTGTTAAAAGTTTTAATTTATTAATTAAGTTTACTCAGACTGCA
AAGTTACGCAAGAGTTTGAAGTGTCCACCCGGAGCCCCCGCCCGAAGGCAG
GGTCGCCCCGGAGGCAACAGAGTCGGACAACAAAGGGTTATGAACATCCCG
GTGGTTAGACCGGGGTCACTTGTAATGATCCCTCCGCAGGTTCACCTACGGA
GG

The chromatogram (Figure 4A) illustrates the high confidence of base identification.

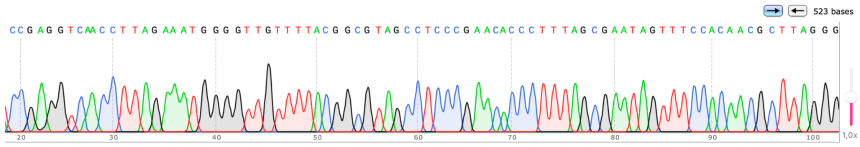

Figure 4A. Chromatogram of the ITS region sequence from *C. cladosporioide.*

Table 1A. BLAST Alignment Results (GenBank)

Sample	**Identified species**	**Identity (%)**	**Query cover (%)**	**Accession number**	**E-value**
Banana/soup	*Penicillium citrinum*	100	98	PV369845	0.0
Banana/soup	*Meyerozyma caribbica*	99.65	98	MG016004	0.0
Banana	*Fusarium verticillioides*	100	94	MN121533	1e-151
Soup	*Cladosporium cladosporioide*	100	99	MF476044	0.0

The high sequence identity (≥99%) and low E-value confirm the species-level identification of the isolates through ITS sequence similarity with GenBank reference entries.